materials

MDPI

Review

Recent Advances in Sodium-Ion Batteries: Cathode Materials

Thang Phan Nguyen and Il Tae Kim *

Department of Chemical and Biological Engineering, Gachon University, Seongnam-si 13120, Gyeonggi-do, Republic of Korea; phanthang87@gmail.com
* Correspondence: itkim@gachon.ac.kr

Abstract: Emerging energy storage systems have received significant attention along with the development of renewable energy, thereby creating a green energy platform for humans. Lithium-ion batteries (LIBs) are commonly used, such as in smartphones, tablets, earphones, and electric vehicles. However, lithium has certain limitations including safety, cost-effectiveness, and environmental issues. Sodium is believed to be an ideal replacement for lithium owing to its infinite abundance, safety, low cost, environmental friendliness, and energy storage behavior similar to that of lithium. Inhered in the achievement in the development of LIBs, sodium-ion batteries (SIBs) have rapidly evolved to be commercialized. Among the cathode, anode, and electrolyte, the cathode remains a significant challenge for achieving a stable, high-rate, and high-capacity device. In this review, recent advances in the development and optimization of cathode materials, including inorganic, organometallic, and organic materials, are discussed for SIBs. In addition, the challenges and strategies for enhancing the stability and performance of SIBs are highlighted.

Keywords: sodium-ion batteries; cathode materials; inorganic cathodes; organic cathodes; Prussian blue analogs

Citation: Nguyen, T.P.; Kim, I.T. Recent Advances in Sodium-Ion Batteries: Cathode Materials. *Materials* **2023**, *16*, 6869. https://doi.org/10.3390/ma16216869

Academic Editors: Giovanni Battista Appetecchi and Satyam Panchal

Received: 5 October 2023
Revised: 23 October 2023
Accepted: 24 October 2023
Published: 26 October 2023

1. Introduction

The invention of batteries has played a key role in the development of miniaturized electrical devices. In particular, the use of lithium-ion batteries (LIBs) allows portable devices to continuously operate with no, or rarely occurring, disruptions [1]. LIBs are currently used in smartphones, tablets, notebooks, and vehicles. The significant achievement of LIBs is owing to the strong activity of lithium-ion insertion and desertion in storage materials with a high specific capacity (approximately 3860 mAh g^{-1}) [2–5]. However, with an increase in capacity, various issues associated with LIBs need to be overcome, including safety, toxicity, and cost-effectiveness [6–10]. Meanwhile, sodium is abundantly available on Earth and has similar properties to lithium in storage devices, which is why it is receiving notable attention [11]. The use of sodium-ion batteries (SIBs) reduces the danger of lithium owing to its strong activation; furthermore, the cost and environmental issues can also be resolved [9,12–22]. Considering the development of LIBs, SIBs have become a promising alternative to LIBs. The working mechanisms of LIBs and SIBs are based on the storage of Li and Na ions in two materials with different potentials separated by an electrolyte, as shown in Figure 1. The insertion and desertion of Na ions in the anode and cathode through the electrolyte create and reduce the potential between the two electrodes, corresponding to charge and discharge processes, respectively. Anode materials can also undergo conversion reactions that react with Na ions, forming alloy states that allow high capacities, such as in expanded graphite (284 mAh g^{-1}), TiO_2-based anodes (200–300 mAh g^{-1}), antimony sulfides (Sb_2S_3) (730 mAh g^{-1}), Sn_4P_3 (>1100 mAh g^{-1}), and phosphorous with a theoretical capacity of ~2596 mAh g^{-1}, among others [23–30]. However, the development of a sodium cathode continues to present limitations such as an unstable and low capacity of 100–200 mAh g^{-1}. SIB cathode materials include a variety of inorganic compounds (metal oxides, phosphates, pyrophosphates, etc.) and organic

or organometallic materials [31,32]. Although achievements have been reported for SIBs and they are being commercialized, the current cathode material has been significantly improved and developed to have better electrochemical properties [33–35].

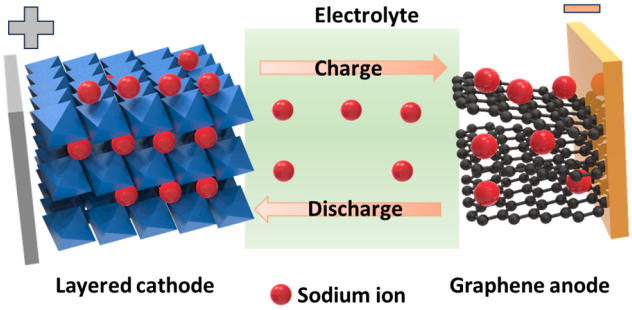

Figure 1. Schematic of the simple operation of a sodium-ion battery employing a layered cathode and graphene anode.

In this review, we provide an overview of the current state of development of SIB cathode materials, including inorganic, organic, and organometallic materials. Recent advances in the development and optimization of these materials have been extensively discussed. In addition, the challenges and strategies related to enhancing the stability and performance of SIBs are highlighted.

2. Review of SIB Cathode Materials

2.1. Inorganic Compounds

2.1.1. Layered Oxide Materials (Na_xMO_2)

The layered oxide materials used for SIBs mostly consist of transition-metal oxides [36]. There are two common phases of $NaMO_2$, which are the O3 and P2 phases, classified based on the different stacking of the oxygen ion frameworks as ABCABCABC (O3) or ABBAABBA (P2), as shown in Figure 2a,b [37,38]. In addition, the O2 phase and birnessite are the layered structures with the tightest and loosest packing, respectively, as shown in Figure 2c,d [39–41]. Among these phases, O3 phase can provide a high Na content and high specific capacity, which enables its application in full cells. However, the degradation of structure during cycling limits its application. To maintain structure, foreign metals with a large ionic radius such as Fe, Cr, Ti, and V can be used introduced [42]. On the other hand, P2 phase has a lower Na content but a wider layer spacing, which leads to faster diffusion of Na^+ ions and improves structural stability during cycling. Similar to LIBs, compounds of Na with Co, Ni, and Mn oxides have layered structures, such as Na_xCoO_2, Na_xNiO_2, and Na_xMnO_2 [43–46]. However, owing to the large size of Na ions, the behavior of CoO_6 or NiO_6 in the lattice with the intercalation of Na varies from that of Li [47]. Na_xCoO_2 and Na_xNiO_2 compounds have exhibited low capacities below or near 100 mAh g^{-1} [48,49]. Reddy et al. fabricated P2-Na_xCoO_2 using the sol–gel method, capable of delivering a capacity of approximately 121 mAh g^{-1} at a rate of 0.1 C [50]. Similarly, $NaNiO_2$ exhibits a capacity of only approximately 80 mAh g^{-1} [51]. Meanwhile, Na_xMnO_2 is a more promising cathode material owing to the multiple oxidation states of the Mn ions in the zigzag layers of the edge-sharing MnO_6; therefore, this cathode exhibits a high theoretical capacity of approximately 240 mAh g^{-1} [52–54]. Na_xMnO_2 can be synthesized from either NaOH and Mn salt or MnO_2. Ma et al. used monoclinic $NaMnO_2$ as a cathode for SIBs and demonstrated a high first discharge capacity of approximately 185 mAh g^{-1} in the 2–3.8 V range [55]. Billaud et al. synthesized β-$NaMnO_2$ which achieved a high capacity of approximately 190 mAh g^{-1} and retained a capacity of 100 mAh g^{-1} after 100 cycles at 2 C [56]. Kubota et al. investigated the effect of the voltage change on distorted O3-phase (O′3) $NaMnO_2$ and found that a phase transition of $NaMnO_2$ occurs above 3.52 V, leading to a decrease in crystallinity, thereby rapidly degrading the capacity during the cycling test [57].

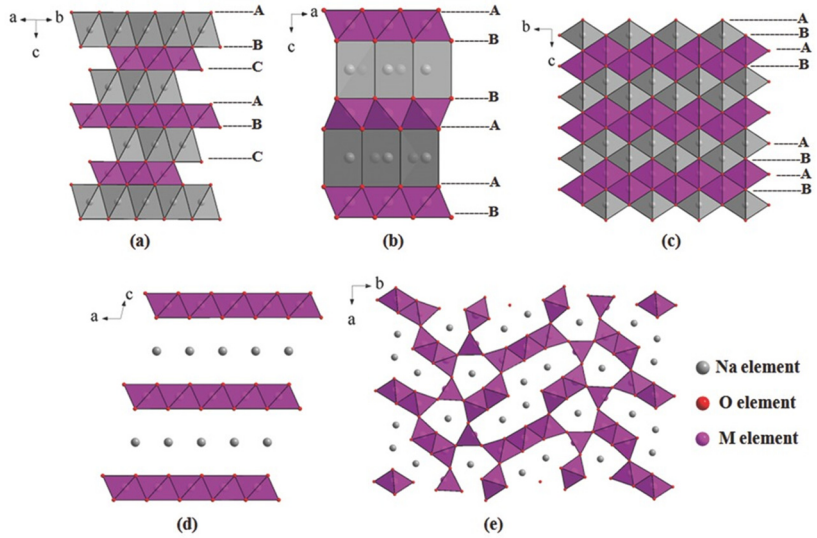

Figure 2. Layered metal oxide: (**a**) O3-phase, (**b**) P2-phase, (**c**) O2-phase, (**d**) birnessite-type layered oxides and (**e**) tunnel oxides. The letters A, B, C are packing patterns of oxygen ions in an abc coordinate system. Reproduced from ref. [37]; Copyright 2015 Wiley-CH.

The drawback of layered materials is their unstable structure in air storage and during cycling; therefore, their capacities can be rapidly or irreversibly degraded [58,59]. Due to its hygroscopic nature, $NaMO_2$ is unstable in air and in moist environments; therefore, its applications are limited. To improve the performance of $NaMnO_2$, the partial replacement of Mn with other metals, such as Li, Ni, Co, Al, Fe, and Zn, has been investigated [60–66]. Kwon et al. proposed the use of a P2-$NaLiMnO_2$ cathode material that exhibited a high reversible capacity of approximately 160 mAh g^{-1} [60]. The insertion of Li ions as dopants led to an inhomogeneous electrostatic repulsion between the Mn and Na ions, thereby enhancing the stability of β-$Na_{0.7}[Mn_{1-x}Li_x]O_{2+y}$, which exhibited a stable cycling capacity for over 120 cycles without a faded capacity. Liu et al. investigated the use of P2-$Na_{2/3}Ni_{1/3}Mn_{2/3}O_2$ as a cathode material for SIBs simply synthesized via a novel sol–gel method (NSG) by employing polystyrene as an additive, as shown in Figure 3a [67]. The main active metal is Ni with Ni^{2+}/Ni^{4+} states that contribute to the redox-pair peaks at a voltage between 3.0–4.0 V and a minor Mn^{3+}/Mn^{4+} redox potential between at 2.0–3.0 V as shown in Figure 3b. Meanwhile, Mn^{4+} effectively maintains the structure of $NaNiMnO_2$, thereby significantly improving its stability. At voltages below 2.0 V, the Mn^{4+} ions were activated and reduced to Mn^{3+}, suffered a disproportional reaction, and dispersed into the electrolyte (Mn^{3+} solid → Mn^{4+} solid → Mn^{2+} electrolyte), and the redox at ~4.0–4.5 V was related to the phase transition from P2 to O2 phase due to the stacking faults, as shown in Figure 3c. Therefore, the material can be rapidly degraded below 2 V. The NSG $Na_{2/3}Ni_{1/3}Mn_{2/3}O_2$ cathode exhibited a reversible capacity of approximately 100 mAh g^{-1} and an excellent rate performance even at rates of 5 C and 10 C, as shown in Figure 3d–f. Nanthagopal et al. used $NaFe_{0.5}Mn_{0.5}O_2$ as a cost-effective SIB cathode material which exhibited a specific capacity of approximately 170 mAh g^{-1} and retained a capacity of approximately 114 mAh g^{-1} after 100 cycles [61]. Liu et al. doped Al ions into $NaMnO_2$ to form P2-$Na_{0.67}Al_{0.1}Mn_{0.9}O_2$ as a SIB cathode material [62]. The strong bonding of Al–O leads to enhanced Na spacing; therefore, Na ions can easily insert and desert into the cathode material. Hence, the presence of Al also reduces the Jahn–Teller effect of the phase transition between P2-P2′, which could cause structural defects and collapse during cycling [68]. Therefore, P2-$NaAl_{0.1}Mn_{0.9}O_2$ can deliver a high capacity of 175 mAh g^{-1} with high stability and rate performance. Replacement with metals such as Ni, Co, Al, and Fe with higher redox states increases the average oxidation state of Mn ions (>3+), which mitigates the structural deterioration resulting from the Jahn–Teller effect and partially increases the redox potential [69]. For example, the redox potential of $Mn^{3+/4+}$ is below

3.0 V, and the partial reduction of Mn^{3+} to Mn^{2+} leads to the dissolution of Mn^{2+} into electrolyte, resulting in structural degradation and reduced capacity. Introducing Fe ions into the structure causes a $Fe^{3+/4+}$ redox between 3.0–4.0 V, increasing the average oxidation state of Mn ions and improving the stability. The higher redox potential of $Fe^{3+/4+}$ also contributes to the working potential of the cathode material. Moreover, Mn and Fe are Earth-abundant elements that promise low-cost and environmentally friendly production. Similar to lithium-based layered metal oxides, the O3 phase of $NaTMnO_x$ (T = Ni, Co, Fe) has a high sodium content and provides a more stable layered oxide, making it applicable to full cells [70,71].

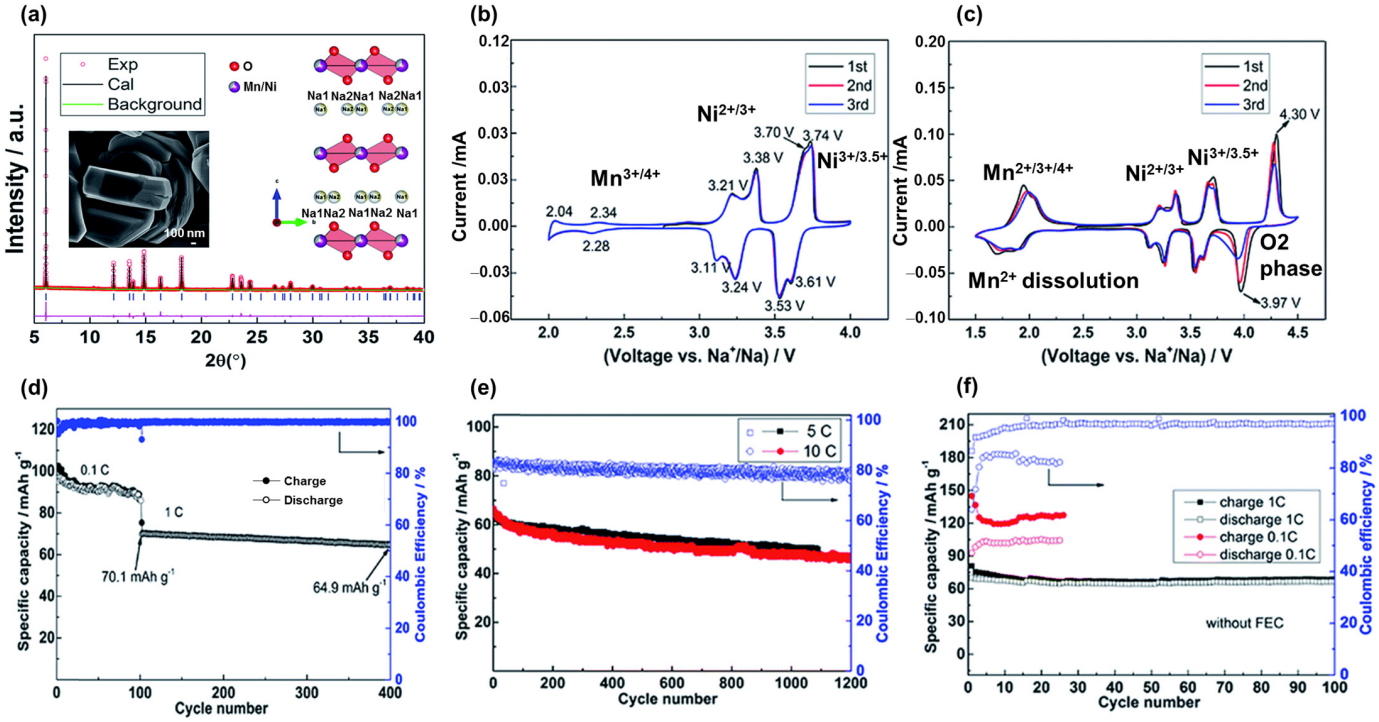

Figure 3. (**a**) X-ray diffraction pattern and inset scanning electron microscopy image of the $Na_{2/3}Ni_{1/3}Mn_{2/3}O_2$ material. Cyclic voltammograms (CVs) at (**b**) 2.0–4.0 V and (**c**) 1.5–4.5 V. Cycling performances at (**d**) 0.1 C and 1 C for 400 cycles, (**e**) 5 C and 10 C for 1200 cycles, and (**f**) of the electrolyte without the additive (FEC). Reproduced with permission from ref. [67]; Copyright 2019 Royal Chemical Society.

A combination of more than three metals was also investigated, including $NaLiNiMnCoO_2$, $NaLiNiMnO_2$, $NaFeMnTiVO_2$, and $NaMnNiCuMgTiO_2$ [72–75]. Kataoka et al. prepared a multi-metal complex of $NaLiNiMnCoO_2$ via co-precipitation and electrochemical ion-exchange methods [72]. The produced $Na_{0.95}Li_{0.15}(Ni_{0.15}Mn_{0.55}Co)O_2$ was then employed as a highly stable cathode which delivered a capacity of greater than 200 mAh g^{-1} for over 40 cycles. Xu et al. investigated the effect of Li ions on $NaLiNiMnO_2$ cathodes in SIBs and determined the importance of each element as follows [74]: The Ni metal was fully oxidized to Ni^{4+} to balance the overall charge of the cell, which also prevented the Jahn–Teller distortion owing to the active Mn^{3+}. Moreover, Ni ions also contributed to the high-voltage redox state of the cathode, widening the range of the working potential from 2.0 to 4.4 V. Li ions were found surrounding Ni^{4+} through NMR resonance methods, which indicated that Li could easily migrate to this material. The remaining Li during cycling enhanced the capacity retention; therefore, this cathode delivered a high reversible capacity of 140 mAh g^{-1} in the 2.0–4.4 V range. Other elements have also been doped to improve the performance of Mn-based cathodes, such as boron-doped $NaLiNiFeMnO_2$, Y-doped P2-type $NaNiMnO_2$, and Mg-doped $NaMnMgO_2$ [76–78].

In addition to Co-, Ni-, and Mn-based metal oxide cathodes, Cr-, Cu-, and Fe-based oxides have also received significant attention [79–84]. Yu et al. developed carbon-coated $NaCrO_2$ as a SIB cathode via an emulsion-drying method that exhibited an excellent performance at a high rate of 50 C with a capacity of approximately 100 mAh g^{-1} [79]. The $NaCrO_2$ cathode also demonstrated significant thermal stability up to 400 °C. At temperatures above 290 °C, instead of oxygen evolution owing to the thermal decomposition, NaCrO2 decomposed to $Na_{0.5}CrO_2$ and CrO_2 phases. Moreover, $Na_{0.5}CrO_2$ continued to exhibit a stable layered structure from the insertion and desertion of the Na ions. Na_xCuO_2 and Na_xFeO_2 also have layered structures and deliver a capacity of approximately 100–200 mAh g^{-1} [80,81,85,86]. Lee et al. found that Fe^{3+}/Fe^{4+} in Na_xFeO_2 was unstable during the redox process, leading to the formation of an octahedral structure, preventing the diffusion of Na ions and degrading the capacity [86]. A typical issue in layered metal oxide materials is the collapse of the structure during the insertion and desertion of sodium ions [37].

2.1.2. Tunnel Oxides

The Na_xMO_2 tunnel oxide consists of M^{4+} and M^{3+} ions at the MO_6 and MO_5 sites, respectively, as illustrated in Figure 2e [87–90]. The mixing of MO_6 and MO_5 creates a tunnel structure that allows Na^+ ions to easily diffuse along the tunnels. This structure was first discovered by Parant et al. (1971) for Na_xMnO_2 ($x < 1$) [91]. It is worth noting that this structure was simply synthesized using various approaches, such as sol–gel, hydrothermal, spray pyrolysis, and microwave-assisted methods [92–95]. $Na_{0.44}MnO_2$ is the most noteworthy tunnel oxide owing to its large tunnels, high theoretical capacity of approximately 121 mAh g^{-1}, and high stability [96,97]. He et al. used a polymer-pyrolysis method to fabricate $Na_{0.44}MnO_2$ nanoplates, which exhibited an outstanding capacity of approximately 96 mAh g^{-1} at a rate of 10 C [98]. However, the capacity of this material could not be improved owing to the fully charged and discharged states of the $Na_{0.22}MnO_2$ and $Na_{0.66}MnO_2$ phases, respectively [96]. Therefore, methods were developed to solve this problem, including cation/anion substitution and surface coating. In cation substitution, Mn^{4+} can be replaced by Ti, Fe, or Zr or by the partial replacement of Na with Li ions [99,100]. Shi et al. doped Zr ions in $Na_{0.44}MNO_2$ as a high-performance SIB cathode, which exhibited a high capacity of approximately 117 mAh g^{-1}; at a high rate of 5 C, the capacity was reversible at approximately 97 mAh g^{-1}, as shown in Figure 4 [101]. Defects at the Na, MnO_6, and MnO_5 sites create Na1 and Na2 in the S-shaped tunnels and Na3 in the smaller pentagonal tunnel, which allows the insertion and desertion of Na, thereby increasing the cycling performance, as illustrated in Figure 4a. As shown in Figure 4b, the insertion and desertion of the Na ions demonstrate six pairs of redox peaks with a small gap between each peak, allowing the rapid diffusion of Na ions. Therefore, the current rate and cycling performances were excellent at 10 C for over 100 cycles, as shown in Figure 4c,d. Zheng et al. used the composition of layered $Na_2Mn_3O_7$ and $Na_{0.44}MnO_2$ as a SIB cathode, which delivered a high specific capacity of approximately 135 mAh g^{-1} and retained a capacity of 88% of the initial state after 100 cycles at 0.2 A g^{-1} [102]. Further improvement remains a challenge for scientists because of the change in structure owing to doping or the substitution of ions such as Co and Al [96]. Zhou et al. used Co-substituted $Na_{0.44}Mn_{1-x}Co_xO_2$ and found that the structure of the tunnel oxide changed to a layered structure [103]. The substitution of Al can form a mixture of the tunnel and layered phases in $NaAl_{0.1}Mn_{0.9}O_2$ SIB cathodes [104]. In comparison to layered oxides, the tunnel oxides provide large channels for diffusion of Na ions, improving conductivity and stability. However, the low content of Na ions in the structure results in low specific capacity (~100 mAh g^{-1}) and energy density. These drawbacks limit commercialization.

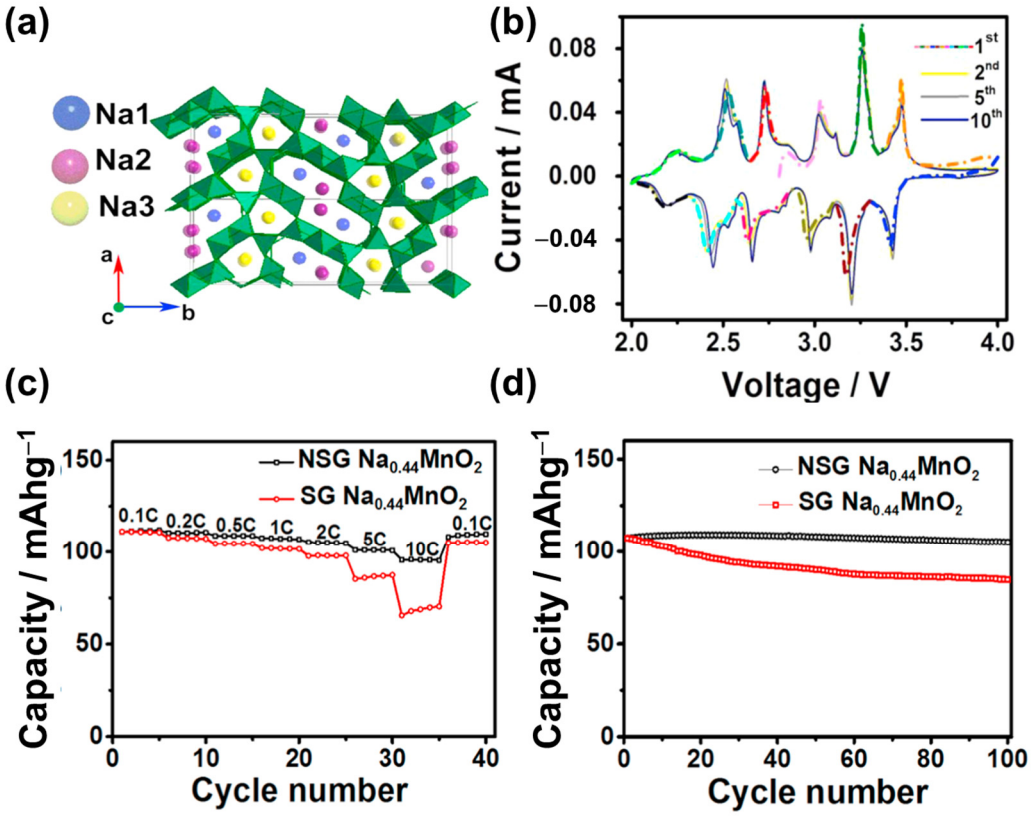

Figure 4. (**a**) Illustration of orthorhombic $Na_{0.44}MnO_2$, (**b**) CV of (novel sol–gel-synthesized) NSG-$Na_{0.44}MnO_2$, (**c**) rate performance at current rates between 0.1–10 C, and (**d**) cycling performances of NSG-$Na_{0.44}MnO_2$ and (conventional sol–gel-synthesized) SG-$Na_{0.44}MnO_2$ at 0.5 C. Reproduced with permission from ref. [98]; Copyright 2016 Elsevier.

2.1.3. Polyanionic Compounds

Phosphate-Based Compound

Polyanionic compounds are generally constructed by a tetrahedral XO_4 group with Na and Me (Fe, V, Co, or Mn) or MeO_x [105–108]. Basically, olivine $NaFePO_4$ consists of tetrahedral PO_4 and octahedral FeO_6 sites, forming a framework that holds Na ions in the lattice or allows the diffusion of Na ions [109]. $NaFePO_4$ is a cost-effective material owing to its abundance of elements and high theoretical capacity of approximately 154 mAh g^{-1}. $NaFePO_4$ exists in two phases: maricite and olivine. The maricite phase is a stable structure with cavities that trap Na ions, preventing their diffusion [105,110]. Meanwhile, the less stable olivine phase has a one-dimensional channel, allowing the diffusion of Na ions through this pathway. Therefore, the olivine phase is more attractive, and improving the stability of this structure with various types of doping has also been investigated [58]. Wang et al. used the DFT simulation method to predict the effect of doping Li into $NaFePO_4$ in both maricite and olivine phases [110]. The results demonstrated that when the Li:Na ratio was above 25%, the olivine phase was more stable than maricite, whereas the presence of Li destabilized the maricite structure. Ali et al. synthesized olivine $NaFePO_4$ via an ion-exchange method from $LiFePO_4$ for SIBs, which was then wrapped with polythiophene (PTh) to enhance the stability of the material [111]. $NaFePO_4$ with PTh experiences the expansion of the insertion and restoration of its structure, which is indicated by the minuscule difference in the unit cell volume (from 320.6 to 320.3 $Å^3$). Therefore, the $NaFePO_4$/PTh cathode exhibits a high reversible capacity of approximately 142 mAh g^{-1}. Altundag et al. used an electrochemical process to exchange Li with Na from $LiFePO_4$ to $NaFePO_4$, which delivered a capacity of approximately 74 mAh g^{-1}. Olivine $NaFePO_4$ structures are promising for SIBs; however, their fabrication remains a major obstacle that requires further investiga-

tion. Maricite $NaCoPO_4$ (red phase) offered a high redox potential of $Co^{2+/3+}$ at 4.0–4.6 V; however, the reversible capacity in a SIB was low at ~35 mAh g^{-1} [107]. Similarly, for $NaMnPO_4$, it was also reported that the specific capacity of maricite phase exhibited a low capacity of ~40 mAh g^{-1} [108]. Priyanka et al. reported a different precursor (Mn) effect for the quality of $NaMnPO_4$. A cathode prepared with a precursor from manganese acetate showed outstanding performance with an initial capacity over 100 mAh g^{-1} [112]. The high performance resulting from the acetate-based Mn precursor could be due to the decomposition of acetate creating a carbon source to enhance the conductivity and porosity of $NaMnPO_4$. Venkatachalam et al. synthesized maricite $NaMnPO_4$ with poly-ethylene glycol (PEG) and diethylene glycol (DEG), which can increase the specific capacity from 50 to ~100 mAh g^{-1} at 0.1 C [113]. The high contribution of carbon sources from PEG and DEG significantly enhanced the conductivity and protected the structure of this material. Phosphate compounds possess a high thermal stability (~600 °C); however, their major drawbacks are low electronic conductivity and low specific capacity, limiting their application in full-cell SIBs [114].

NASICON

A Na super-ionic conductor (NASICON) can be used as an electrolyte and electrode material owing to its 3D-open framework of $Na_xM_2(PO_4)_3$ (M = V, Fe, Ti, Nb, Zr) [115]. NASICON comprises MO_6 and PO_4 polyhedral sites in a framework that creates large channels for Na diffusion. This structure was first proposed by Hong and Goodenough in a $Na_{1+x}Zr_2P_{3-x}Si_xO_{12}$ compound (P can be replaced by Si, S, Mo, and As) [116,117]. Owing to its high stability, high Na conductivity, and wide electrochemical windows (1.85–4.9 V vs. Na/Na^+), NASICON is also applied as a solid electrolyte in SIBs [118]. The ion exchange of Zr^{4+} with Li^+, K^+, and Ag^+ was first performed, while Si^{4+} was stabilized in the structure. As a complete NASICON with three full Na ions, $Na_3V_2(PO_4)_3$ (NVP) quickly received significant attention as a promising candidate material for providing a high probability of sodium insertion and desertion [119,120]. NVP has a theoretical capacity of ~117.6 mAh g^{-1} and a high redox voltage range of 3.3–3.4 V [121]. Therefore, with the modification process including the addition of conductive carbonaceous materials, NVP conductivity can be enhanced, exhibiting a notable rate performance [122]. Song et al. used a carbothermal reduction method to fabricate NVP, which exhibited a high capacity of approximately 117 mAh g^{-1} [123]. Cao et al. synthesized high-crystalline M-NVP/C nanoparticles using MIL-101 as the V source combined with an amorphous carbon layer, as shown in Figure 5a–c [124]. The M-NVP/C cathode delivered a high capacity of approximately 136 mAh g^{-1} and an excellent performance at high current rates of 1 C, 5 C, and 10 C for 1000 cycles, as shown in Figure 5d–h. In addition, the substitutions of Na, V, and P were found to be effective in improving its stability [125–127]. Lim et al. used the sol–gel method to produce $Na_{3-x}K_xV_2(PO_4)_3/C$ [125]. The use of K ions helped increase the Na-ion diffusion pathway and improved the stability and rate performance of NVP. Meanwhile, Mg replaced the V ions and improved the conductivity of the material; $Mg_{0.07}$-NVP delivered a reversible capacity of approximately 113 mAh g^{-1} at 0.1 C and a high reversible capacity of 95 mAh g^{-1} at 10 C [127]. Pal et al. used Si-doped NVP as a replacement for P to form $Na_{3.1}V_2(PO_4)_{2.9}(SiO_4)_{0.1}$, which delivered an initial capacity of approximately 112 mAh g^{-1} and enhanced the capacity in comparison to NVP at high rates [126]. Fluorine is also favorable for substitution in the PO_4 group owing to the larger ionicity of the metal when bonded with F compared to O. Moreover, F atoms were found to be compatible with the PO_4 group in polyanionic compounds; therefore, the fluorine phosphate compound is believed to enhance the diffusion of Na^+ ions [128]. Song et al. fabricated $Na_3V_2(PO_4)_2F_3$ via a carbothermal reduction method as a SIB cathode material [129]. The existence of F in NVP changes the electrochemical behavior from a single redox couple at 3.06/3.72 V to a double redox couple at 3.24/3.91 and 3.83/4.26 V; therefore, the specific power density is improved.

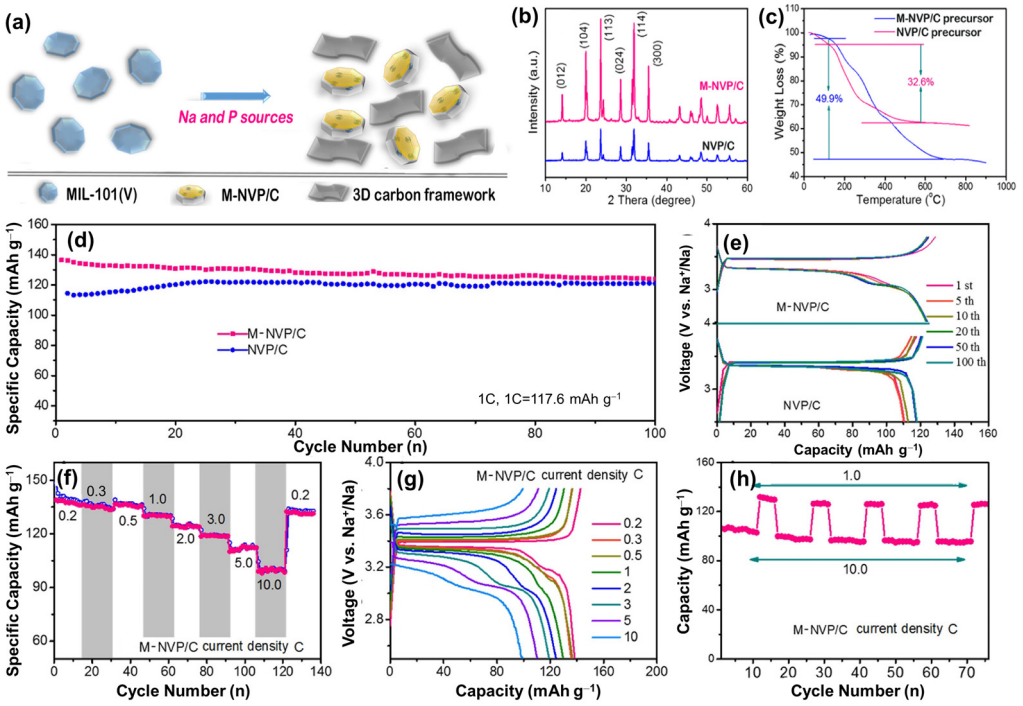

Figure 5. (**a**) M-NVP/C synthesis scheme, (**b**) XRD, (**c**) thermogravimetric analysis plots, (**d**) cycling performance at 1 C, (**e**) voltage profiles of M-NVP and NVP/C; (**f**) rate performance, (**g**) voltage profiles at different C rates ranging from 0.2 C–10 C, and (**h**) rate performance at 1 C and 10 C of the M-NVP cathode. Reproduced with permission from ref. [124]; Copyright 2019 Elsevier.

2.1.4. Pyrophosphates

Pyrophosphate $Na_xMP_2O_7$ consists of MO_6 (M = V, Fe, Mn, Co, Ni) sites and a P_2O_7 group (interconnected PO_4–PO_4) that forms a framework with Na ions [130–135]. This framework allows the diffusion of Na ions; therefore, it is also a stable cathode material for SIBs. Barpanda et al. revealed that $Na_2FeP_2O_7$ was constructed by corner-sharing FeO_6–FeO_6 to form Fe_2O_{11}, which combines with the P_2O_7 group to form a triclinic structure [136]. After calcination at temperatures above 560 °C, the triclinic $Na_2PeP_2O_7$ transformed into a monoclinic phase, which improved the stability of this material during cycling. Kim et al. used the defect engineering of Na in $Na_2CoP_2O_7$ to produce a high-voltage cathode for SIBs [137]. The deficiency of the Na-stabilized structure of $Na_{2-x}CoP_2O_7$ ($x > 0.2$) was also found in Fe, Ni, and Mg pyrophosphates, such as $Na_{1.66}Fe_{1.17}P_2O_7$, $Na_{1.82}Ni_{1.09}P_2O_7$, and $Na_{1.82}Mg_{1.09}P_2O_7$ [138–141]. Specifically, $Na_{2-x}Co_2P_2O_7$ ($x > 0.2$) achieved a high average voltage of approximately 4.3 V versus Na/Na^+ with a specific capacity of approximately 80 mAh g^{-1}. Owing to the similar roles of the V, Fe, Mn, Co, and Ni transition metals in the structure, the replacement of a cheaper metal such as Fe and the improvement of the voltage by using Co and Ni in other pyrophosphate materials were investigated. Liu et al. investigated the use of $Na_2Mn_{3-x}Fex(P_2O_7)_2$ as a SIB cathode and revealed that the diffusion coefficient of Na ions improved by two orders of magnitude with $x > 0.5$ [142]; however, the capacity remained low at approximately 86 mAh g^{-1}. Deng et al. fabricated a high-Na-content $Na_7V_3(P_2O_7)_4$, which was also used as a high-voltage SIB cathode at an average voltage of approximately 4.0 V with a capacity of approximately 80 mAh g^{-1}. Kumar et al. proposed the use of $Mo_2P_2O_{11}$ as a SIB cathode with a high capacity of approximately 90 mAh g^{-1} [143]. The structure of $Mo_2P_2O_{11}$ is also a framework of MoO_6 sites with PO_4 and P_2O_7 sites. Therefore, incomplete or shared atoms can form a tunnel phase in phosphates. Pyrophosphate-based cathode materials remain limited owing to their low capacity because the P_2O_7 group is large; therefore, the replacement of this group with PO_4 and F could be an efficient method to enhance their capacity and stability [131,144,145]. Pu et al. fabricated a $Na_4Fe_3(PO_4)_2P_2O_7/C$ nanosphere for SIB

cathodes, which delivered a high capacity of approximately 128 mAh g^{-1} at 0.2 C and a remarkable rate performance at 100 C with a capacity of >70 mAh g^{-1} [144]. Kundu et al. used fluorine to modify pyrophosphates and produced $Na_4NiP_2O_7F_2$ as a high-voltage cathode for SIBs [145]. The presence of strong electronegative F^- groups incorporated with P–O moieties increased the redox of Ni^{2+}/Ni^{4+} owing to the high-charge region between 4.7 and 5.2 V. However, this material was not sufficiently stable to retain the capacity of the SIBs.

2.1.5. Silicates

Silicate compounds, such as lithium orthosilicate Li_2FeSiO_4 with a theoretical capacity of approximately 300 mAh g^{-1}, generally have a higher theoretical capacity than other polyanions owing to their low molecular weight [146]. Similar to Li_2FeSiO_4, the sodium silicate Na_2MSiO_4 compound consists of MO_4 (M = Fe, Ni, Mn, Co) and SiO_4 sites, forming a framework that allows the diffusion of Na ions [147–149]. Silicates were previously popular in the glass industry owing to their high thermal and physical stabilities [150]. Co/Fe-compound sodium silicates were predicted to exhibit anti-site-exchange behavior, promising to be stable electrode materials [151,152]. Na_2FeSiO_4 is the most promising silicate compound, having a high theoretical capacity of approximately 276 mAh g^{-1} [153]. Kee et al. fabricated Na_2FeSiO_4 using a solvothermal method as a SIB cathode material, which exhibited a high initial capacity of approximately 126 mAh g^{-1} [154]. However, the material's capacity quickly degrades owing to the collapse of the crystal into an amorphous structure. Meanwhile, Na_2CoSiO_4 demonstrated a better stability; however, its capacity was approximately 100–120 mAh g^{-1} [148,149,155]. Guan et al. resolved the stability issue of Na_2FeSiO_4 by introducing a fluorine dopant, which delivered a high capacity of approximately 270 mAh g^{-1} as a SIB cathode [156]. The presence of fluorine with strong electronegativity reduced the strain of the Na-hosting cathode, and the volume change during the charge and discharge process was only approximately 1.38%. Law et al. prepared Na_2MnSiO_4 that delivered a high capacity of approximately 210 mAh g^{-1} at 0.1 C and a reversible capacity of ~100 mAh g^{-1} at 5 C [157]. The excellent performance of Na_2MnSiO_4 was achieved owing to the additional vinylene carbonate in the electrolyte, which allowed the formation of a passivated layer during cycling, as shown in Figure 6. Therefore, the drawback of an unstable structure can be resolved by using a protective layer or surface passivation.

2.2. Organic Compounds

The development of flexible devices and environmentally friendly materials has encouraged the application of organic compounds as cathode materials in energy storage systems, such as LIBs and SIBs [158]. Ranging from small molecules to high-molecular polymers, organic materials are promising for applications in green renewable energy in the future. For example, the molecular structure of $Na_4C_8H_2O_6$ (2,5-dihydroxyterephthalic acid, NaDTA) was investigated as a SIB cathode material at working potential windows of approximately 1.6–2.8 V versus Na/Na^+ and delivered a high capacity of approximately 180 mAh g^{-1} [159]. NaDTA can also be used as an anode material with a capacity greater than 200 mAh g^{-1} owing to it binding up to six Na ions [160]. Kim et al. demonstrated the use of $C_6Cl_4O_2$ (tetrachloro-1,4-benzoquinone) in a porous carbon template as a cathode of SIBs, as illustrated in Figure 7a,b [161]. The carbon skeleton-supported $C_6Cl_4O_2$ cathode exhibited a high initial capacity of approximately 160 mAh g^{-1} and an average voltage of approximately 2.72 V, as shown in Figure 7c. Wang et al. produced a polymer from perylene 3,4,9,10-tetracarboxylic dianhydride, pyromellitic dianhydride (PMDA), and 1,4,5,8-naphthalenetetracarboxylic dianhydride, which contained C=O bindings, providing interactions with Na^+ ions as a cathode for SIBs, as illustrated in Figure 7d [159]. This polymer demonstrated a high reversible capacity of approximately 150 mAh g^{-1} at a working voltage of 1.5–3.5 V and a long lifetime of over 5000 cycles, retaining 87.5% of the capacity in comparison to the initial cycle, as shown in Figure 7e,f. Shen et al. fabricated

poly(diphenylaminesulfonic acid sodium) as a SIB cathode material, which delivered a reversible capacity of approximately 100 mAh g^{-1} at a high potential of 3.6 V versus Na/Na^+ [162]. Wang et al. proposed an extended π-conjugated structure in sodium 4,4′-stilbene-dicarboxylate (SSDC) to provide an increased charge transport, which could easily enhance the rate performance of this organic cathode material in SIB by up to 10 A g^{-1} [163]. Organic cathodes can also be based on the insertion of anions such as ClO_4^-. Han et al. employed non-crystalline oligopyrene as a SIB cathode material, which is based on the insertion of ClO_4^- [164]. During cycling, pyrene was oxidized and reduced, allowing the interaction with charged ClO_4^-; therefore, each pyrene unit could store ClO_4^- anions. As a SIB cathode, oligopyrene exhibits a high theoretical reversible capacity of approximately 134 mAh g^{-1}. Sakaushi et al. fabricated a dicyanobenzene-based aromatic porous honeycomb (APH) cathode with two types of storage mechanisms [165]. APH can store Na+ ions at voltages below 2.8 V. When the voltage is higher than 2.8 V, the APH cathode exhibits a p-doped region, which allows the insertion of ClO^{4-} anions [165]. Therefore, APH has a wide working potential of 1.3–4.1 V versus Na/Na^+ and a high reversible capacity greater than 120 mAh g^{-1} at 0.1 A g^{-1}. Due to the electronic insulative nature of organic materials, they show a low conductivity, limiting their high rate performance. To overcome this limitation, cathode materials should contain high amount of carbon materials (30–60 wt%) to achieve a high rate performance [159,160,162,163,165].

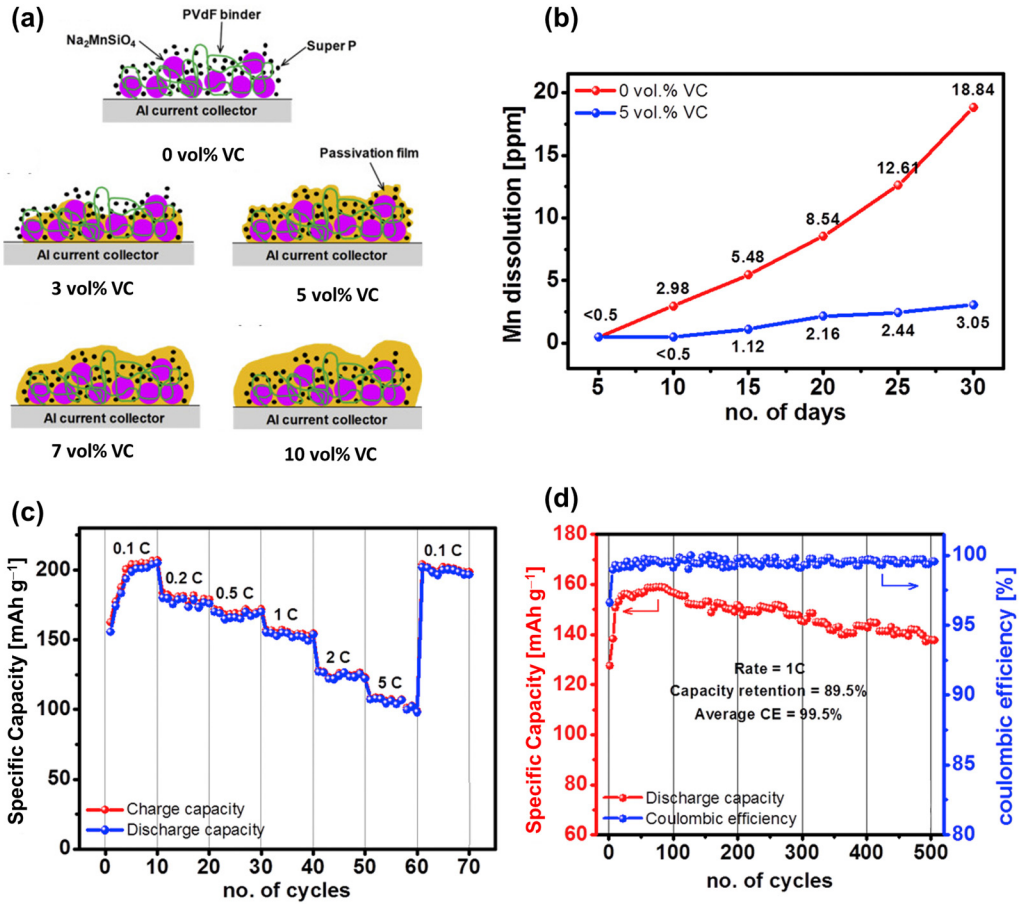

Figure 6. (**a**) Illustration of the passivated layer on the Na_2MnSiO_4 cathode with additive vinylene carbonate (VC). (**b**) Mn dissolution of the Na_2MnSiO_4 electrode in electrolytes at room temperature. (**c**) Rate and (**d**) cycling performances of Na_2MnSiO_4 with 5 vol% VC at 1 C. Reproduced from ref. [157]; Copyright 2017 Elsevier.

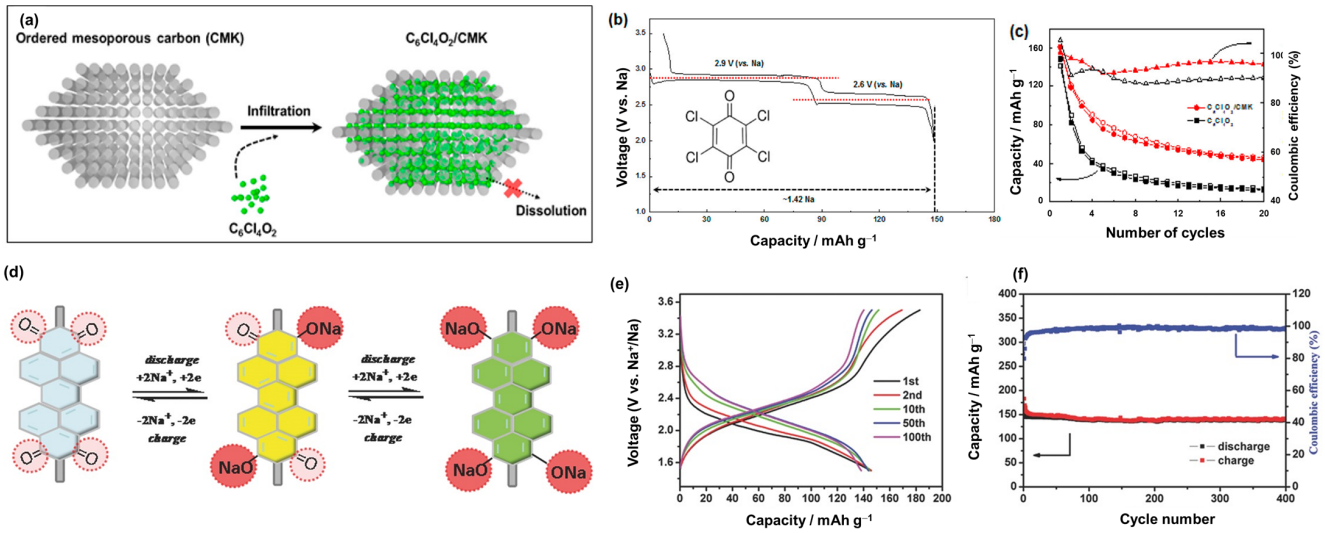

Figure 7. (**a**) $C_6Cl_4O_2$/CMK synthesis scheme, (**b**) voltage profiles of $C_6Cl_4O_2$ at 10 mA g^{-1}, and (**c**) cycling performance of $C_6Cl_4O_2$ with and without CMK. Reproduced with permission from ref. [161]; Copyright 2015 American Chemical Society. (**d**) Schematic diagram of the redox mechanism, (**e**) voltage profiles, and (**f**) cycling performance of PTCDA-based PIs at 0.1 C. Reproduced with permission from ref. [159]; Copyright 2014 Wiley-CH.

2.3. Metal–Organic Compounds: Prussian Blue Analogs

The combination of inorganic and organic structures has received considerable attention owing to the advantages of both material types [166]. Inorganic materials have a stable structure and high conductivity, whereas organic materials are eco-friendly, easy to process, and safe to use. Recently, the development of organometallic materials in framework structures has introduced an advanced technique for material design, enabling the discovery of new composite properties for metals and organics. Metal–organic frameworks (MOF) can form a tremendous structure from various metal–organic compounds, providing large channels that allow the capture of ions or molecules; therefore, they have been used in various applications, including drug delivery, catalysis, and energy storage [167–169]. Simple and famous MOFs used for energy storage are Prussian blue analogs (PBAs), which are alkaline metal ferrocyanides $A_xMFe(CN)_6$ (A = Na, K; M = Fe, Mn, Co, Ni, Cu) [170]. The CN, Fe, and M matrices create a cage-like structure, holding the Na and K ions. PBAs generally exhibit a face-centered cubic structure (Fm3-m) [171–173]. The performance of PBAs in SIBs is based on the redox reactions of Fe^{2+}/Fe^{3+} and the metal M, believed to have a high theoretical capacity of approximately 170 mAh g^{-1} for SIBs [174]. The basic PBA, which is $Na_4Fe(CN)_6$, contains the highest number of Na ions; however, it is a soluble compound that is easily degraded during cycling [175,176]. Therefore, Yang et al. demonstrated a solid solution of $Na_4Fe(CN)_6$/NaCl in a SIB that exhibited a capacity of approximately 75 mAh g^{-1} [177]. Qian et al. prepared a composition of $Na_4Fe(CN)_6$ with carbon, which also functioned as a SIB cathode [175]. By replacing Na ions with transition metals, the PBA structures were stabilized and widely used in SIBs [178]. Sun et al. used Fe^{3+} to form $Fe_4[Fe(CN)_6]_3$ for a SIB cathode, which delivered a high capacity of approximately 146 mAh g^{-1} at 20 mA g^{-1} [179]. However, the rate performance and stability remained low; therefore, various types of transition metals, such as Ni, Cu, Mn, and V, have been used to create more stable and high-conductivity cathodes [180–182]. Song et al. fabricated $Na_2MnFe(CN)_6$ (Mn-PBA) and found that the removal of water molecules from the material significantly improved its performance, as shown in Figure 7 [183]. Mn-PBA and other PBAs naturally have monoclinic (Na-rich) or cubic structures that are partially supported by water molecules in their crystals. After removing the water molecules, Mn-PBA changed into a distorted framework or rhombohedral structure. Owing to the irreversibility of the monoclinic phase to the cubic phase, the Na per unit was reduced. Hence, the Jahn–Teller

distortion of Mn^{3+} led to the degradation of the structure, thereby reducing the capacity, as illustrated in Figure 8a. It is worth noting that the rhombohedral phase allows the Na^+ ions to be captured more efficiently; therefore, the water-removed Mn-PBA cathode enhanced the electrochemical performance, delivering a high capacity of approximately 150 mAh g^{-1} and a high rate performance even at 20 C, as shown in Figure 8b–d. However, dried Mn-PBA quickly absorbs water molecules; therefore, its fabrication and application remain limited. Hu et al. investigated the effect of Ni replacement in Mn-PBA as a SIB cathode [184]. Ni with a 10% replacement of Mn in Mn-PBA can enhance stability, delivering a capacity of approximately 110 mAh g^{-1} and a high rate performance. Xu et al. proposed a scalable preparation of Mn/Ni-PBA that delivered a capacity of approximately 100 mAh g^{-1} and an excellent rate performance, even at 100 C [185]. In particular, they reported that the activation in the first cycle at 4.8 V could significantly stabilize the structure, improving the cycling performance of the cathode. The presence of V, Co, and Ti increased the working potential of the PBA [186–189]. Takachi et al. used $Na_xCo[Fe(CN)_6]_{0.9}$ as a SIB cathode, which delivered a capacity of approximately 135 mAh g^{-1} and demonstrated high-voltage redox couples of approximately 3.4 and 3.8 V versus Na/Na^+ [190]. Baster reported that the replacement of Fe^{2+} with V^{2+} ions to form vanadium hexacyanoferrate (NaVHCF) exhibited a redox potential of ~2.3/3.6 V versus Na/Na^+ [191]. Meanwhile, the presence of V–O binding in sodium vanadium hexacyanoferrate (NaVHCF) as a SIB cathode demonstrated only one redox potential [187]. Nguyen et al. reported that the presence of V–O passivated the high-spin Fe related to the low redox potential, supporting the structure of the low-spin Fe ion; therefore, NaVHCF provided a single redox potential of approximately 3.26/3.65 V versus Na/Na^+ [192]. However, the capacity was only approximately 70–80 mAh g^{-1}.

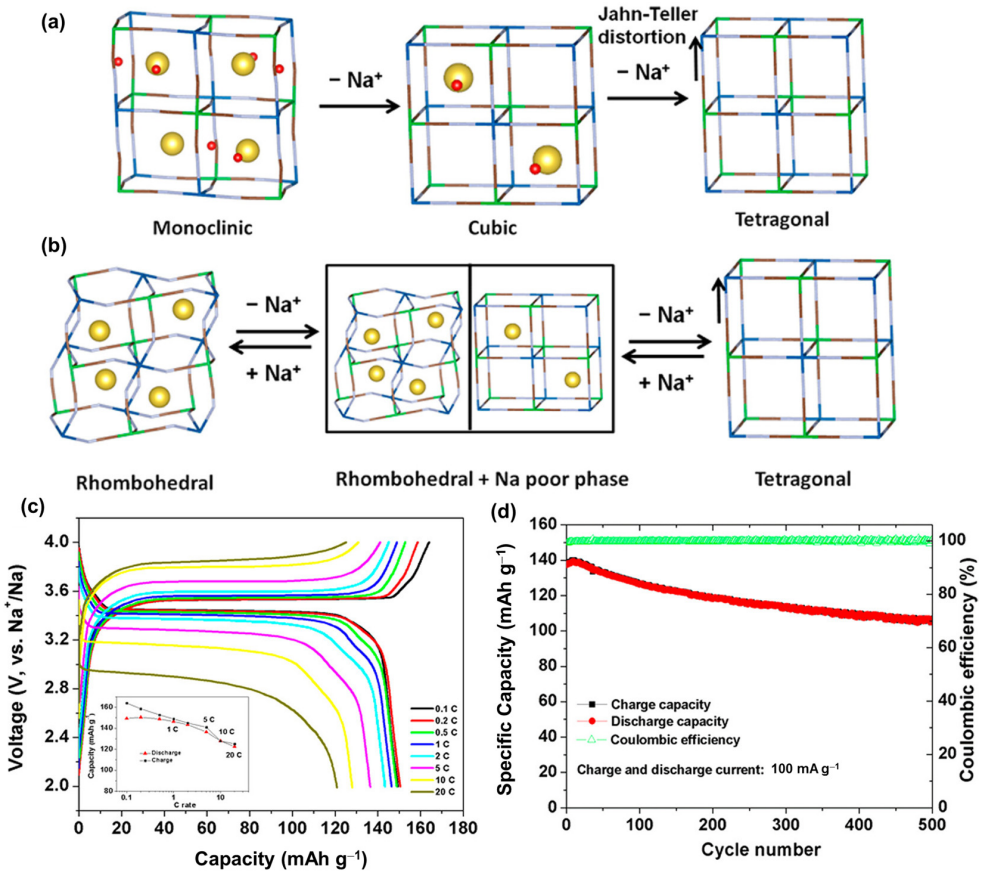

Figure 8. (**a**) Schematic of the monoclinic, cubic M-PBA and (**b**) rhombohedral M-PBA with the insertion and desertion of Na^+ ions. (**c**) Voltage profiles at different rates from 0.1–20 C and the (**d**) cycling performance of the rhombohedral M-PBA. Reproduced with permission from ref. [183]; Copyright 2015 American Chemical Society.

Other MOFs have received considerable attention as anode materials owing to their new structures and stable redox potentials [193]. However, the application to SIBs as cathode materials remains limited, which may be owing to the fact that a high-voltage cathode is difficult to obtain, and the selection of large organic groups can lead to a decrease in conductivity [194]. In addition, the MOF structure can be used as a template to form oxide, nitride, carbide, and sulfide materials as anode materials in SIBs and for the design of cathode materials [195]. Li et al. used MIL-53(Al) to dope Al into Na_2FePO_4/C as a SIB cathode, where MIL-53(Al) was used as a template to form a porous structure with a carbon cover [196]. It delivered a high capacity of approximately 115 mAh g^{-1} [196] with stable cyclability.

3. Discussion

LIBs have become popular in portable devices, vehicles, and energy storage systems for renewable energy. With the development of LIBs, a variety of cathode materials for SIBs have also recently evolved as listed in Table 1. Owing to the abundance of Na, SIBs are believed to be an ideal replacement for LIBs. As shown in Figure 9, each type of cathode material has its advantages and disadvantages. For instance, layered metal oxides have a high capacity and low cost but are sensitive to moisture and structural degradation. Prussian blue is more stable but the effect of water molecules in the structure affects its performance. Organic cathode materials have a good flexibility and stable redox potential but their lower conductivity, thermal stability, and dissolvability in the electrolyte should be resolved. Therefore, the advantages and disadvantages of each practical condition should be carefully considered. To improve their performance, the approach methods were also varied for each type of material. Due to an instability in structure of layered metal oxide cathodes, they were fast degraded during cycling. To stabilize structural stability, inactive metals such as V, Mg, Zn, and Ca can be doped to the lattice, or anions like F can be added [197,198]. Considering a tunnel metal oxide, control of the tunnel size optimizes its capacity. Meanwhile, for polyanionic compounds such as NASICON or other phosphate-based compounds, defect engineering can be considered, including metal- and F-doping methods [199]. Silicate compounds are low-cost and eco-friendly metal sources, and their high capacity needs to improve the structural stability before commercialization [154]. The surfaces of inorganic compounds can be passivated using a carbon-coating method that not only enhances their conductivity but also protects against the effects of humidity or expansion during the insertion of Na ions. The stability of Prussian blue and other organometallic compounds can be enhanced by using a host material such as Ni foam or a porous carbon skeleton [200]. Organic materials can be designed to have a good structure to enhance capacity and conductivity but they remain in the activation group with C=O, C=C, or C=N. Sulfurization and other cross-linking methods can also be considered to yield better combinations [201]. In addition, the use of additives in the electrolyte is another approach to enhance stability, in which the solid electrolyte interface from cycling can be used as a protective layer [202]. Along with the development of electrode materials and electrolytes, SIBs have been commercialized with layered oxides, polyanions, and Prussian blue types [32]. These materials are simple to manufacture (hydrothermal, co-precipitation method, etc.) and inexpensive, and they mainly use Mn and Fe metals and add Ni, Zn, or Mg, to increase stability, and conductive carbon is introduced for air stability and structural protection. Organic materials with low thermal stability and conductivity are utilized for some specific purposes that require biocompatible and/or specified applications. Therefore, it is considered that most of the developed materials have the potential to be commercialized if SIBs can solve current issues such as cost-effectiveness, high capacity, high stability, and high rate performance.

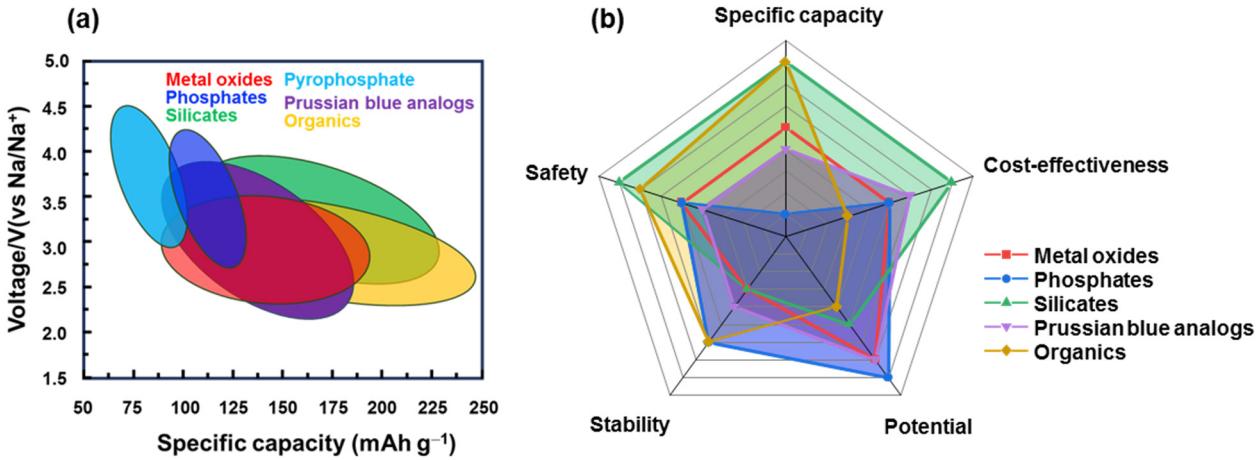

Figure 9. Comparison of SIB cathode materials' (**a**) specific capacity and working potential; (**b**) specific capacity, cost-effectiveness, potential, stability, and safety issues.

Table 1. Summary of SIB cathode materials.

Materials	Redox Couple	Working Voltage (V)	Current Density	Specific Capacity (mAh g^{-1})	Ref.
LAYERED OXIDES					
$Na_{0.7}CoO_2$	Co^{3+}/Co^{4+}	2.0–3.5	0.08 C	70.4	[48]
Na_xCoO_2	Co^{3+}/Co^{4+}	2.0–4.0	0.1 C	121	[50]
$Na_{0.44}Mn_{1-x}Co_xO_2$	Co^{3+}/Co^{4+} Mn^{3+}/Mn^{4+}	2.0–4.2	0.1 C	220	[103]
$NaFeO_2$	Fe^{3+}/Fe^{4+}	2.0–3.6	0.15 C	101	[86]
$NaTi_{0.5}Ni_{0.5}O_2$	Ni^{2+}/Ni^{3+} Ti^{3+}/Ti^{4+}	2.0–3.8	0.23 C	130	[203]
$NaFe_{0.5}Ni_{0.5}O_2$	Ni^{3+}/Ni^{4+} Fe^{2+}/Fe^{3+}	2.0–3.8	0.24 C	125	[203]
$NaNiO_2$	Ni^{2+}/Ni^{3+}	1.25–3.75	0.02 C	120	[49]
Na_2NiO_2	Ni^{3+}/Ni^{4+}	2.0–3.6	0.05 C	89	[51]
$NaCrO_2$:Na_2NiO_2	Ni^{3+}/Ni^{4+} Cr^{2+}/Cr^{3+}	2.0–3.6	0.05 C	107	[51]
$NaMnO_2$	Mn^{2+}/Mn^{3+}	2–3.8	0.05 C	185	[55]
β-$NaMnO_2$	Mn^{3+}/Mn^{4+}	2–4.2	0.05 C	190	[56]
$Na_{0.7}MnO_2$	Mn^{3+}/Mn^{4+}	2.0–4.5	0.25 C	163	[43]
$Na_{0.67}Mn_{0.85}Al_{0.15}O_2$	Mn^{3+}/Mn^{4+}	2.0–4.0	0.05 C	104	[63]
$Na_2/_3Ni_1/_3Mn_2/_3O_2$	Mn^{3+}/Mn^{4+} Ni^{3+}/Ni^{4+}	2.0–4.0	0.1 C	89	[67]
$Na_{0.7}Mn_{0.93}Li_{0.07}O_2$	Mn^{3+}/Mn^{4+}	2.0–3.8	0.4 C	183	[60]
$Na_{0.95}Li_{0.15}(Ni_{0.15}Mn_{0.55}Co_{0.1})O_2$	Mn^{3+}/Mn^{4+} Ni^{3+}/Ni^{4+}	2.0–4.2	0.05 C	200	[72]
$Na_{0.80}[Li_{0.12}Ni_{0.22}Mn_{0.66}]O_2$	Mn^{3+}/Mn^{4+} Ni^{3+}/Ni^{4+}	2.0–4.0	0.1 C	120	[74]
$Na_{0.67}Ni_{0.33}Mn_{0.67}Y_{0.02}O_2$	Mn^{3+}/Mn^{4+} Ni^{3+}/Ni^{4+}	2.0–4.5	0.05 C	137	[77]

Table 1. *Cont.*

Materials	Redox Couple	Working Voltage (V)	Current Density	Specific Capacity (mAh g^{-1})	Ref.
TUNNEL OXIDES					
$Na_{0.44}MnO_2$	Mn^{3+}/Mn^{4+}	2.0–4.0	10 C	96	[87]
$Na_{0.44}Mn_{0.98}Zr_{0.02}O_2$	Mn^{3+}/Mn^{4+}	2.0–3.8	0.1 C	117	[101]
$Na_{0.44}MnO_2{\cdot}Na_2Mn_3O_7$	Mn^{3+}/Mn^{4+}	1.5–4.6	1.37 C	145	[102]
$Na_{2/3}Mn_{0.95}Mg_{0.05}O_2$	Mn^{3+}/Mn^{4+}	1.5–4.0	7 C	140	[78]
POLYANION COMPOUNDS					
$NaFePO_4$	Fe^{2+}/Fe^{3+}	2.2–4.0	0.07 C	142	[111]
$Na_3V_2(PO_4)_3$	V^{3+}/V^{4+} V^{2+}/V^{3+}	2.0–4.6	0.1 C	117.6	[123]
Na_3-x$KxV_2(PO_4)_3/C$	V^{3+}/V^{4+} V^{2+}/V^{3+}	2.5–3.8	0.2 C	~110	[125]
$Na_3V_{1.93}Mg_{0.07}(PO_4)_3/C$	V^{3+}/V^{4+} V^{2+}/V^{3+}	2.3–4.6	0.1 C	113.5	[127]
$Na_{3.1}V_2(PO_4)_{2.9}(SiO_4)_{0.1}/C$	V^{3+}/V^{4+} V^{2+}/V^{3+}	2.5–4.0	0.1 C	112	[126]
$Na_3V_2(PO_4)_2F_3$	V^{3+}/V^{4+} V^{2+}/V^{3+}	2.0–4.6	0.1 C	117	[129]
PYROPHOSPHATES					
$Na_{3.32}Fe_{2.34}(P_2O_7)_2$	Fe^{2+}/Fe^{3+}	1.7–4.0	0.05 C	117.6	[138]
$Na_2FeP_2O_7$	Fe^{2+}/Fe^{3+}	2.0–4.5	0.05 C	90	[141]
$Na_2CoP_2O_7$	Co^{2+}/Co^{3+}	1.6–4.5	0.05 C	80	[134]
$Na_2MnP_2O_7$	Mn^{3+}/Mn^{4+}	2.0–4.45	0.05 C	80	[135]
$Na_4NiP_2O_7F_2$	$Ni^{2+}/Ni^{3+}/Ni^{4+}$	3.0–5.5	0.01 C	50	[145]
Na_2Mn_3-x$Fex(P_2O_7)_2$	Fe^{2+}/Fe^{3+} Mn^{3+}/Mn^{4+}	1.5–4.5	0.058 C	86.8	[142]
$Na_4Fe_3(PO_4)_2P_2O_7/C$	Fe^{2+}/Fe^{3+}	1.5–4.2	0.2 C	128.5	[144]
Silicates					
Na_2FeSiO_4	$Fe^{2+}/Fe^{3+}/Fe^{4+}$	1.5–4.5	0.1 C	271	[157]
Na_2MnSiO_4	Mn^{3+}/Mn^{4+}	2.0–4.3	0.1 C	210	[146]
Na_2CoSiO_4	Co^{2+}/Co^{3+}	1.5–4.0	0.05 C	112	[156]
Na_2CoSiO_4/CNT	Co^{2+}/Co^{3+}	1.5–4.0	0.05 C	125	[156]
Organic materials					
$Na_4C_8H_2O_6$	$Na_2C_8H_2O_6/Na_4C_8H_2O_6$	1.6–2.8	0.1 C	180	[159]
PTCDA based Polyimides	Na_2PI/Na_4PI	1.5–3.5	0.2 C	112	[160]
NTCDA based Polyimides	Na_2PI/Na_4PI	1.5–3.5	0.2 C	125	[160]
PMDA based Polyimides	Na_2PI/Na_4PI	1.5–3.5	0.2 C	133	[160]
Poly(diphenylaminesulfonic acid sodium) (PDS)	-	2.5–4.2	0.5 C	100	[162]
Bipolar porous organic electrode	-	1.3–4.1	0.05 C	200	[165]

Table 1. *Cont.*

Materials	Redox Couple	Working Voltage (V)	Current Density	Specific Capacity (mAh g^{-1})	Ref.
Prussian blue analogs					
$Na_4Fe(CN)_6/NaCl$	Fe^{2+}/Fe^{3+}	1.5–3.9	0.93 C	75	[177]
$Na_4Fe(CN)_6/C$	Fe^{2+}/Fe^{3+}	2.0–4.0	0.1 C	90	[175]
$Na_2MnFe(CN)_6$	Mn^{2+}/Mn^{3+}	2.0–4.0	0.1 C	150	[183]
$NaxMn_{0.5}Ni_{0.5}Fe(CN)_6$	Mn^{2+}/Mn^{3+}	2.0–4.0	0.1 C	100	[185]
$NaxCo[Fe(CN)_6]_{0.9}$	Fe^{2+}/Fe^{3+} Co^{2+}/Co^{3+}	2.0–4.0	0.6 C	135	[185]
$NaxVOFe(CN)_6$	Fe^{2+}/Fe^{3+}	2.0–4.0	0.25 C	65	[187]

In summary, this review reveals the current developments in SIB cathode materials, such as layered metal oxides, tunnel metal oxides, phosphate-based compounds, organic compounds, Prussian blue analogs, and organometallic compounds. Many methods including anion/cation doping, composition, defect engineering, and structural design of SIB cathodes demonstrate their significant development to be comparable with LIBs. However, the development of SIBs can be further investigated to optimize the process or engineer the structure and design of cathode materials with high capacity, high voltage potential, and long life.

Author Contributions: T.P.N.: conceptualization, visualization, writing, review, and editing. I.T.K.: Project administration, funding acquisition, review, and editing. All authors have read and agreed to the published version of the manuscript.

Funding: This study was supported by a National Research Foundation of Korea (NRF) grant funded by the Korean government (MSIT) (NRF-2022R1F1A1062928). This research was also supported by the Basic Science Research Capacity Enhancement Project through a Korea Basic Science Institute (National Research Facilities and Equipment Center) grant funded by the Ministry of Education (2019R1A6C1010016).

Institutional Review Board Statement: Not applicable.

Informed Consent Statement: Not applicable.

Data Availability Statement: Not applicable.

Conflicts of Interest: The authors declare no conflict of interest.

References

1. Mahmud, S.; Rahman, M.; Kamruzzaman, M.; Ali, M.O.; Emon, M.S.A.; Khatun, H.; Ali, M.R. Recent advances in lithium-ion battery materials for improved electrochemical performance: A review. *Results Eng.* **2022**, *15*, 100472. [CrossRef]
2. Liu, J.; Bao, Z.N.; Cui, Y.; Dufek, E.J.; Goodenough, J.B.; Khalifah, P.; Li, Q.Y.; Liaw, B.Y.; Liu, P.; Manthiram, A.; et al. Pathways for practical high-energy long-cycling lithium metal batteries. *Nat. Energy* **2019**, *4*, 180–186. [CrossRef]
3. Boebinger, M.G.; Yarema, O.; Yarema, M.; Unocic, K.A.; Unocic, R.R.; Wood, V.; McDowell, M.T. Spontaneous and reversible hollowing of alloy anode nanocrystals for stable battery cycling. *Nat. Nanotechnol.* **2020**, *15*, 475–481. [CrossRef] [PubMed]
4. Masias, A.; Marcicki, J.; Paxton, W.A. Opportunities and Challenges of Lithium Ion Batteries in Automotive Applications. *ACS Energy Lett.* **2021**, *6*, 621–630. [CrossRef]
5. Walter, M.; Kovalenko, M.V.; Kravchyk, K.V. Challenges and benefits of post-lithium-ion batteries. *New J. Chem.* **2020**, *44*, 1677–1683. [CrossRef]
6. Zhang, W.; Zhang, F.; Ming, F.; Alshareef, H.N. Sodium-ion battery anodes: Status and future trends. *EnergyChem* **2019**, *1*, 100012. [CrossRef]
7. Li, X.F.; Dhanabalan, A.; Gu, L.; Wang, C.L. Three-Dimensional Porous Core-Shell Sn@Carbon Composite Anodes for High-Performance Lithium-Ion Battery Applications. *Adv. Energy Mater.* **2012**, *2*, 238–244. [CrossRef]
8. Hatzell, K.B.; Chen, X.C.; Cobb, C.L.; Dasgupta, N.P.; Dixit, M.B.; Marbella, L.E.; McDowell, M.T.; Mukherjee, P.P.; Verma, A.; Viswanathan, V.; et al. Challenges in Lithium Metal Anodes for Solid-State Batteries. *ACS Energy Lett.* **2020**, *5*, 922–934. [CrossRef]

9. Velumani, D.; Bansal, A. Thermal Behavior of Lithium- and Sodium-Ion Batteries: A Review on Heat Generation, Battery Degradation, Thermal Runway—Perspective and Future Directions. *Energy Fuels* **2022**, *36*, 14000–14029. [CrossRef]
10. Ponnada, S.; Kiai, M.S.; Krishnapriya, R.; Singhal, R.; Sharma, R.K. Lithium-Free Batteries: Needs and Challenges. *Energy Fuels* **2022**, *36*, 6013–6026. [CrossRef]
11. Abraham, K.M. How Comparable Are Sodium-Ion Batteries to Lithium-Ion Counterparts? *ACS Energy Lett.* **2020**, *5*, 3544–3547. [CrossRef]
12. Mosallanejad, B.; Malek, S.S.; Ershadi, M.; Daryakenari, A.A.; Cao, Q.; Boorboor Ajdari, F.; Ramakrishna, S. Cycling degradation and safety issues in sodium-ion batteries: Promises of electrolyte additives. *J. Electroanal. Chem.* **2021**, *895*, 115505. [CrossRef]
13. Ellis, B.L.; Nazar, L.F. Sodium and sodium-ion energy storage batteries. *Curr. Opin. Solid. State Mater. Sci.* **2012**, *16*, 168–177. [CrossRef]
14. Liu, Q.; Zhao, X.; Yang, Q.; Hou, L.; Mu, D.; Tan, G.; Li, L.; Chen, R.; Wu, F. The Progress in the Electrolytes for Solid State Sodium-Ion Battery. *Adv. Mater. Technol.* **2023**, *8*, 2200822. [CrossRef]
15. Åvall, G.; Mindemark, J.; Brandell, D.; Johansson, P. Sodium-Ion Battery Electrolytes: Modeling and Simulations. *Adv. Energy Mater.* **2018**, *8*, 1703036. [CrossRef]
16. Wang, B.; Wang, X.; Liang, C.; Yan, M.; Jiang, Y. An All-Prussian-Blue-Based Aqueous Sodium-Ion Battery. *ChemElectroChem* **2019**, *6*, 4848–4853. [CrossRef]
17. Palomares, V.; Casas-Cabanas, M.; Castillo-Martínez, E.; Han, M.H.; Rojo, T. Update on Na-based battery materials: A growing research path. *Energy Environ. Sci.* **2013**, *6*, 2312–2337. [CrossRef]
18. Li, Y.; Wu, F.; Li, Y.; Liu, M.; Feng, X.; Bai, Y.; Wu, C. Ether-based electrolytes for sodium ion batteries. *Chem. Soc. Rev.* **2022**, *51*, 4484–4536. [CrossRef]
19. Wang, X.; Roy, S.; Shi, Q.; Li, Y.; Zhao, Y.; Zhang, J. Progress in and application prospects of advanced and cost-effective iron (Fe)-based cathode materials for sodium-ion batteries. *J. Mater. Chem. A* **2021**, *9*, 1938–1969. [CrossRef]
20. Lee, J.M.; Singh, G.; Cha, W.; Kim, S.; Yi, J.; Hwang, S.-J.; Vinu, A. Recent Advances in Developing Hybrid Materials for Sodium-Ion Battery Anodes. *ACS Energy Lett.* **2020**, *5*, 1939–1966. [CrossRef]
21. Tian, Y.; Zeng, G.; Rutt, A.; Shi, T.; Kim, H.; Wang, J.; Koettgen, J.; Sun, Y.; Ouyang, B.; Chen, T.; et al. Promises and Challenges of Next-Generation "Beyond Li-Ion" Batteries for Electric Vehicles and Grid Decarbonization. *Chem. Rev.* **2021**, *121*, 1623–1669. [CrossRef]
22. Hwang, J.-Y.; Myung, S.-T.; Sun, Y.-K. Sodium-ion batteries: Present and future. *Chem. Soc. Rev.* **2017**, *46*, 3529–3614. [CrossRef]
23. Wen, Y.; He, K.; Zhu, Y.; Han, F.; Xu, Y.; Matsuda, I.; Ishii, Y.; Cumings, J.; Wang, C. Expanded graphite as superior anode for sodium-ion batteries. *Nat. Commun.* **2014**, *5*, 4033. [CrossRef]
24. He, J.; Wei, Y.; Zhai, T.; Li, H. Antimony-based materials as promising anodes for rechargeable lithium-ion and sodium-ion batteries. *Mater. Chem. Front.* **2018**, *2*, 437–455. [CrossRef]
25. Yu, D.Y.W.; Prikhodchenko, P.V.; Mason, C.W.; Batabyal, S.K.; Gun, J.; Sladkevich, S.; Medvedev, A.G.; Lev, O. High-capacity antimony sulphide nanoparticle-decorated graphene composite as anode for sodium-ion batteries. *Nat. Commun.* **2013**, *4*, 2922. [CrossRef]
26. Hwang, J.-Y.; Du, H.-L.; Yun, B.-N.; Jeong, M.-G.; Kim, J.-S.; Kim, H.; Jung, H.-G.; Sun, Y.-K. Carbon-Free TiO_2 Microspheres as Anode Materials for Sodium Ion Batteries. *ACS Energy Lett.* **2019**, *4*, 494–501. [CrossRef]
27. Ni, J.; Li, L.; Lu, J. Phosphorus: An Anode of Choice for Sodium-Ion Batteries. *ACS Energy Lett.* **2018**, *3*, 1137–1144. [CrossRef]
28. Durai, L.; Gopalakrishnan, A.; Badhulika, S. Solid-state synthesis of β-$NaAlO_2$ nanoflakes as an anode material for high-performance sodium-ion batteries. *Mater. Chem. Front.* **2022**, *6*, 2913–2920. [CrossRef]
29. Nam, K.-H.; Hwa, Y.; Park, C.-M. Zinc Phosphides as Outstanding Sodium-Ion Battery Anodes. *ACS Appl. Mater. Interfaces* **2020**, *12*, 15053–15062. [CrossRef]
30. Xu, H.; Chen, H.; Gao, C. Advanced Graphene Materials for Sodium/Potassium/Aluminum-Ion Batteries. *ACS Mater. Lett.* **2021**, *3*, 1221–1237. [CrossRef]
31. He, M.; Davis, R.; Chartouni, D.; Johnson, M.; Abplanalp, M.; Troendle, P.; Suetterlin, R.-P. Assessment of the first commercial Prussian blue based sodium-ion battery. *J. Power Sources* **2022**, *548*, 232036. [CrossRef]
32. Yadav, P.; Shelke, V.; Patrike, A.; Shelke, M. Sodium-based batteries: Development, commercialization journey and new emerging chemistries. *Oxf. Open Mater. Sci.* **2022**, *3*, itac019. [CrossRef]
33. Wang, M.; Wang, Q.; Ding, X.; Wang, Y.; Xin, Y.; Singh, P.; Wu, F.; Gao, H. The prospect and challenges of sodium-ion batteries for low-temperature conditions. *Interdiscip. Mater.* **2022**, *1*, 373–395. [CrossRef]
34. Zhao, L.; Zhang, T.; Li, W.; Li, T.; Zhang, L.; Zhang, X.; Wang, Z. Engineering of Sodium-Ion Batteries: Opportunities and Challenges. *Engineering*, 2022; *in press*. [CrossRef]
35. Xie, J.; Gu, P.; Zhang, Q. Nanostructured Conjugated Polymers: Toward High-Performance Organic Electrodes for Rechargeable Batteries. *ACS Energy Lett.* **2017**, *2*, 1985–1996. [CrossRef]
36. Zuo, W.; Innocenti, A.; Zarrabeitia, M.; Bresser, D.; Yang, Y.; Passerini, S. Layered Oxide Cathodes for Sodium-Ion Batteries: Storage Mechanism, Electrochemistry, and Techno-economics. *Acc. Chem. Res.* **2023**, *56*, 284–296. [CrossRef]
37. Xiang, X.; Zhang, K.; Chen, J. Recent Advances and Prospects of Cathode Materials for Sodium-Ion Batteries. *Adv. Mater.* **2015**, *27*, 5343–5364. [CrossRef]

38. Stansby, J.H.; Sharma, N.; Goonetilleke, D. Probing the charged state of layered positive electrodes in sodium-ion batteries: Reaction pathways, stability and opportunities. *J. Mater. Chem. A* **2020**, *8*, 24833–24867. [CrossRef]
39. Jiang, L.; Dong, M.; Dou, Y.; Chen, S.; Liu, P.; Yin, H.; Zhao, H. Manganese oxides transformed from orthorhombic phase to birnessite with enhanced electrochemical performance as supercapacitor electrodes. *J. Mater. Chem. A* **2020**, *8*, 3746–3753. [CrossRef]
40. Luo, J.; Huang, A.; Park, S.H.; Suib, S.L.; O'Young, C.-L. Crystallization of Sodium-Birnessite and Accompanied Phase Transformation. *Chem. Mater.* **1998**, *10*, 1561–1568. [CrossRef]
41. Chen, S.; Liao, Z.; Kang, J.; Zhang, Y.; Zhi, S.; Cai, X.; Yang, W.; Zou, H.; Yang, W. Enhanced cyclic performance of O_2-type Mn-based layered oxide via Al doping for lithium-ion battery. *J. Alloys Compd.* **2022**, *910*, 164793. [CrossRef]
42. Song, T.; Chen, L.; Gastol, D.; Dong, B.; Marco, J.F.; Berry, F.; Slater, P.; Reed, D.; Kendrick, E. High-Voltage Stabilization of O_3-Type Layered Oxide for Sodium-Ion Batteries by Simultaneous Tin Dual Modification. *Chem. Mater.* **2022**, *34*, 4153–4165. [CrossRef] [PubMed]
43. Su, D.; Wang, C.; Ahn, H.-J.; Wang, G. Single Crystalline $Na_{0.7}MnO_2$ Nanoplates as Cathode Materials for Sodium-Ion Batteries with Enhanced Performance. *Chem. Eur. J.* **2013**, *19*, 10884–10889. [CrossRef] [PubMed]
44. Shibata, T.; Fukuzumi, Y.; Kobayashi, W.; Moritomo, Y. Fast discharge process of layered cobalt oxides due to high Na^+ diffusion. *Sci. Rep.* **2015**, *5*, 9006. [CrossRef] [PubMed]
45. Li, G.; Zhu, W.; Liu, W. First-principles calculations of the Ti-doping effects on layered $NaNiO_2$ cathode materials for advanced Na-ion batteries. *J. Indian. Chem. Soc.* **2022**, *99*, 100424. [CrossRef]
46. Kanwade, A.; Gupta, S.; Kankane, A.; Tiwari, M.K.; Srivastava, A.; Kumar Satrughna, J.A.; Chand Yadav, S.; Shirage, P.M. Transition metal oxides as a cathode for indispensable Na-Ion batteries. *RSC Adv.* **2022**, *12*, 23284–23310. [CrossRef] [PubMed]
47. Heubner, C.; Matthey, B.; Lein, T.; Wolke, F.; Liebmann, T.; Lämmel, C.; Schneider, M.; Herrmann, M.; Michaelis, A. Insights into the electrochemical Li/Na-exchange in layered $LiCoO_2$ cathode material. *Energy Stor. Mater.* **2020**, *27*, 377–386. [CrossRef]
48. Rai, A.K.; Anh, L.T.; Gim, J.; Mathew, V.; Kim, J. Electrochemical properties of Na_xCoO_2 (x~0.71) cathode for rechargeable sodium-ion batteries. *Ceram. Int.* **2014**, *40*, 2411–2417. [CrossRef]
49. Vassilaras, P.; Ma, X.; Li, X.; Ceder, G. Electrochemical Properties of Monoclinic $NaNiO_2$. *J. Electrochem. Soc.* **2013**, *160*, A207. [CrossRef]
50. Rami Reddy, B.V.; Ravikumar, R.; Nithya, C.; Gopukumar, S. High performance Na_xCoO_2 as a cathode material for rechargeable sodium batteries. *J. Mater. Chem. A* **2015**, *3*, 18059–18063. [CrossRef]
51. Park, K.; Yu, B.-C.; Goodenough, J.B. Electrochemical and Chemical Properties of Na_2NiO_2 as a Cathode Additive for a Rechargeable Sodium Battery. *Chem. Mater.* **2015**, *27*, 6682–6688. [CrossRef]
52. Chen, T.; Ouyang, B.; Fan, X.; Zhou, W.; Liu, W.; Liu, K. Oxide cathodes for sodium-ion batteries: Designs, challenges, and perspectives. *Carbon. Energy* **2022**, *4*, 170–199. [CrossRef]
53. Zhang, R.; Lu, Z.; Yang, Y.; Shi, W. First-principles investigation of the monoclinic $NaMnO_2$ cathode material for rechargeable Na-ion batteries. *Curr. Appl. Phys.* **2018**, *18*, 1431–1435. [CrossRef]
54. Palluzzi, M.; Silvestri, L.; Celeste, A.; Tuccillo, M.; Latini, A.; Brutti, S. Structural Degradation of O3-$NaMnO_2$ Positive Electrodes in Sodium-Ion Batteries. *Crystals* **2022**, *12*, 885. [CrossRef]
55. Ma, X.; Chen, H.; Ceder, G. Electrochemical Properties of Monoclinic $NaMnO_2$. *J. Electrochem. Soc.* **2011**, *158*, A1307. [CrossRef]
56. Billaud, J.; Clément, R.J.; Armstrong, A.R.; Canales-Vázquez, J.; Rozier, P.; Grey, C.P.; Bruce, P.G. β-$NaMnO_2$: A High-Performance Cathode for Sodium-Ion Batteries. *J. Am. Chem. Soc.* **2014**, *136*, 17243–17248. [CrossRef]
57. Kubota, K.; Miyazaki, M.; Kim, E.J.; Yoshida, H.; Barpanda, P.; Komaba, S. Structural change induced by electrochemical sodium extraction from layered O′3-$NaMnO_2$. *J. Mater. Chem. A* **2021**, *9*, 26810–26819. [CrossRef]
58. Xiao, J.; Li, X.; Tang, K.; Wang, D.; Long, M.; Gao, H.; Chen, W.; Liu, C.; Liu, H.; Wang, G. Recent progress of emerging cathode materials for sodium ion batteries. *Mater. Chem. Front.* **2021**, *5*, 3735–3764. [CrossRef]
59. Gupta, P.; Pushpakanth, S.; Haider, M.A.; Basu, S. Understanding the Design of Cathode Materials for Na-Ion Batteries. *ACS Omega* **2022**, *7*, 5605–5614. [CrossRef]
60. Kwon, M.-S.; Lim, S.G.; Park, Y.; Lee, S.-M.; Chung, K.Y.; Shin, T.J.; Lee, K.T. P2 Orthorhombic $Na_{0.7}[Mn_{1-x}Li_x]O_{2+y}$ as Cathode Materials for Na-Ion Batteries. *ACS Appl. Mater. Interfaces* **2017**, *9*, 14758–14768. [CrossRef]
61. Nanthagopal, M.; Ho, C.W.; Shaji, N.; Sim, G.S.; Varun Karthik, M.; Kim, H.K.; Lee, C.W. Enhanced $NaFe_{0.5}Mn_{0.5}O_2$/C Nanocomposite as a Cathode for Sodium-Ion Batteries. *Nanomaterials* **2022**, *12*, 984. [CrossRef]
62. Liu, X.; Zuo, W.; Zheng, B.; Xiang, Y.; Zhou, K.; Xiao, Z.; Shan, P.; Shi, J.; Li, Q.; Zhong, G.; et al. P2-$Na_{0.67}Al_xMn_{1-x}O_2$: Cost-Effective, Stable and High-Rate Sodium Electrodes by Suppressing Phase Transitions and Enhancing Sodium Cation Mobility. *Angew. Chem. Int. Ed.* **2019**, *58*, 18086–18095. [CrossRef]
63. Abou-Rjeily, J.; Bezza, I.; Laziz, N.A.; Neacsa, D.; Autret-Lambert, C.; Ghamouss, F. P2-$Na_{0.67}Mn_{0.85}Al_{0.15}O_2$ and $NaMn_2O_4$ Blend as Cathode Materials for Sodium-Ion Batteries Using a Natural β-MnO_2 Precursor. *ACS Omega* **2021**, *6*, 1064–1072. [CrossRef]
64. Shi, Q.; Qi, R.; Feng, X.; Wang, J.; Li, Y.; Yao, Z.; Wang, X.; Li, Q.; Lu, X.; Zhang, J.; et al. Niobium-doped layered cathode material for high-power and low-temperature sodium-ion batteries. *Nat. Commun.* **2022**, *13*, 3205. [CrossRef]
65. Zuo, W.; Liu, X.; Qiu, J.; Zhang, D.; Xiao, Z.; Xie, J.; Ren, F.; Wang, J.; Li, Y.; Ortiz, G.F.; et al. Engineering Na^+-layer spacings to stabilize Mn-based layered cathodes for sodium-ion batteries. *Nat. Commun.* **2021**, *12*, 4903. [CrossRef] [PubMed]

66. Clément, R.J.; Bruce, P.G.; Grey, C.P. Review—Manganese-Based P2-Type Transition Metal Oxides as Sodium-Ion Battery Cathode Materials. *J. Electrochem. Soc.* **2015**, *162*, A2589. [CrossRef]
67. Liu, Q.; Hu, Z.; Chen, M.; Zou, C.; Jin, H.; Wang, S.; Gu, Q.; Chou, S. P2-type $Na_{2/3}Ni_{1/3}Mn_{2/3}O_2$ as a cathode material with high-rate and long-life for sodium ion storage. *J. Mater. Chem. A* **2019**, *7*, 9215–9221. [CrossRef]
68. Zheng, L.; Wang, Z.; Wu, M.; Xu, B.; Ouyang, C. Jahn–Teller type small polaron assisted Na diffusion in $NaMnO_2$ as a cathode material for Na-ion batteries. *J. Mater. Chem. A* **2019**, *7*, 6053–6061. [CrossRef]
69. Nathan, M.G.T.; Yu, H.; Kim, G.-T.; Kim, J.-H.; Cho, J.S.; Kim, J.; Kim, J.-K. Recent Advances in Layered Metal-Oxide Cathodes for Application in Potassium-Ion Batteries. *Adv. Sci.* **2022**, *9*, 2105882. [CrossRef]
70. Xu, J.; Liu, H.; Meng, Y.S. Exploring Li substituted O3-structured layered oxides $NaLi_xNi_{1/3-x}Mn_{1/3+x}Co_{1/3-x}O_2$ (x = 0.07, 0.13, and 0.2) as promising cathode materials for rechargeable Na batteries. *Electrochem. Commun.* **2015**, *60*, 13–16. [CrossRef]
71. Liu, H.; Xu, J.; Ma, C.; Meng, Y.S. A new O3-type layered oxide cathode with high energy/power density for rechargeable Na batteries. *Chem. Commun.* **2015**, *51*, 4693–4696. [CrossRef]
72. Kataoka, R.; Mukai, T.; Yoshizawa, A.; Sakai, T. Development of High Capacity Cathode Material for Sodium Ion Batteries $Na_{0.95}Li_{0.15}(Ni_{0.15}Mn_{0.55}Co_{0.1})O_2$. *J. Electrochem. Soc.* **2013**, *160*, A933–A939. [CrossRef]
73. Banik, T.; Bhattacharya, I. Novel P2-Type $Na_{0.66}Fe_{0.5-2x}Mn_{0.5}Ti_xV_xO_2$ Cathode for High-Capacity. In *Electrochemical Society Meeting Abstracts 240*; MA2021-02; The Electrochemical Society, Inc.: Pennington, NJ, USA, 2021; p. 238. [CrossRef]
74. Xu, J.; Lee, D.H.; Clément, R.J.; Yu, X.; Leskes, M.; Pell, A.J.; Pintacuda, G.; Yang, X.-Q.; Grey, C.P.; Meng, Y.S. Identifying the Critical Role of Li Substitution in P2–$Na_x[Li_yNi_zMn_{1-y-z}]O_2$ (0 < x, y, z < 1) Intercalation Cathode Materials for High-Energy Na-Ion Batteries. *Chem. Mater.* **2014**, *26*, 1260–1269. [CrossRef]
75. Fu, F.; Liu, X.; Fu, X.; Chen, H.; Huang, L.; Fan, J.; Le, J.; Wang, Q.; Yang, W.; Ren, Y.; et al. Entropy and crystal-facet modulation of P2-type layered cathodes for long-lasting sodium-based batteries. *Nat. Commun.* **2022**, *13*, 2826. [CrossRef]
76. Guo, Y.-J.; Wang, P.-F.; Niu, Y.-B.; Zhang, X.-D.; Li, Q.; Yu, X.; Fan, M.; Chen, W.-P.; Yu, Y.; Liu, X.; et al. Boron-doped sodium layered oxide for reversible oxygen redox reaction in Na-Ion battery cathodes. *Nat. Commun.* **2021**, *12*, 5267. [CrossRef]
77. Kim, S.; Min, K.; Park, K. Y-doped P2-type $Na_{0.67}Ni_{0.33}Mn_{0.67}O_2$: A sodium-ion battery cathode with fast charging and enhanced cyclic performance. *J. Alloys Compd.* **2021**, *874*, 160027. [CrossRef]
78. Clément, R.J.; Billaud, J.; Robert Armstrong, A.; Singh, G.; Rojo, T.; Bruce, P.G.; Grey, C.P. Structurally stable Mg-doped P2-$Na_{2/3}Mn_{1-y}Mg_yO_2$ sodium-ion battery cathodes with high rate performance: Insights from electrochemical, NMR and diffraction studies. *Energy Environ. Sci.* **2016**, *9*, 3240–3251. [CrossRef]
79. Yu, C.-Y.; Park, J.-S.; Jung, H.-G.; Chung, K.-Y.; Aurbach, D.; Sun, Y.-K.; Myung, S.-T. $NaCrO_2$ cathode for high-rate sodium-ion batteries. *Energy Environ. Sci.* **2015**, *8*, 2019–2026. [CrossRef]
80. Yabuuchi, N.; Yoshida, H.; Komaba, S. Crystal Structures and Electrode Performance of Alpha-$NaFeO_2$ for Rechargeable Sodium Batteries. *Electrochemistry* **2012**, *80*, 716–719. [CrossRef]
81. Ono, Y.; Yui, Y.; Hayashi, M.; Asakura, K.; Kitabayashi, H.; Takahashi, K.I. Electrochemical Properties of $NaCuO_2$ for Sodium-Ion Secondary Batteries. *ECS Trans.* **2014**, *58*, 33–39. [CrossRef]
82. Liang, J.; Liu, L.; Liu, X.; Meng, X.; Zeng, L.; Liu, J.; Li, J.; Shi, Z.; Yang, Y. O3-Type $NaCrO_2$ as a Superior Cathode Material for Sodium/Potassium-Ion Batteries Ensured by High Structural Reversibility. *ACS Appl. Mater. Interfaces* **2021**, *13*, 22635–22645. [CrossRef]
83. Myung, S.-T.; Park, J.s.; Jung, H.-G.; Chung, K.Y.; Aurbach, D.; Yu, C.-y.; Sun, Y.-K. $NaCrO_2$ Cathode for High-Rate Sodium-Ionbatteries. In *Electrochemical Society Meeting Abstracts 230*; MA2016-02; The Electrochemical Society, Inc.: Pennington, NJ, USA, 2016; p. 664. [CrossRef]
84. Wang, Z.; Shaw, L. Doping of $NaCrO_2$ Cathode Material to Enhance Electrochemical Performance for Sodium-Ion Batteries. In *Electrochemical Society Meeting Abstracts 239*; MA2021-01; The Electrochemical Society, Inc.: Pennington, NJ, USA, 2021; p. 356. [CrossRef]
85. Ono, Y. Structural Analysis of $NaCuO_2$ Cathode at Various Charged/Discharged Stages and Its Reaction Mechanism. *Electrochemistry* **2018**, *86*, 309–314. [CrossRef]
86. Lee, E.; Brown, D.E.; Alp, E.E.; Ren, Y.; Lu, J.; Woo, J.-J.; Johnson, C.S. New Insights into the Performance Degradation of Fe-Based Layered Oxides in Sodium-Ion Batteries: Instability of Fe^{3+}/Fe^{4+} Redox in α-$NaFeO_2$. *Chem. Mater.* **2015**, *27*, 6755–6764. [CrossRef]
87. Feng, J.; Luo, S.; Cai, K.; Yan, S.; Wang, Q.; Zhang, Y.; Liu, X. Research progress of tunnel-type sodium manganese oxide cathodes for SIBs. *Chin. Chem. Lett.* **2022**, *33*, 2316–2326. [CrossRef]
88. Byles, B.; Pomerantseva, E. Stabilization of Tunnel Manganese Oxide Electrodes in Li-Ion and Na-Ion Batteries. In *Electrochemical Society Meeting Abstracts 233*; MA2018-01; The Electrochemical Society, Inc.: Pennington, NJ, USA, 2018; p. 2581. [CrossRef]
89. Wang, Y.; Liu, J.; Lee, B.; Qiao, R.; Yang, Z.; Xu, S.; Yu, X.; Gu, L.; Hu, Y.-S.; Yang, W.; et al. Ti-substituted tunnel-type $Na_{0.44}MnO_2$ oxide as a negative electrode for aqueous sodium-ion batteries. *Nat. Commun.* **2015**, *6*, 6401. [CrossRef]
90. Oz, E.; Altin, S.; Avci, S. Tunnel/Layer Composite $Na_{0.44}MnO_2$ Cathode Material with Enhanced Structural Stability via Cobalt Doping for Sodium-Ion Batteries. *ACS Omega* **2023**, *8*, 27170–27178. [CrossRef]
91. Parant, J.-P.; Olazcuaga, R.; Devalette, M.; Fouassier, C.; Hagenmuller, P. Sur quelques nouvelles phases de formule Na_xMnO_2 ($x \leq 1$). *J. Solid. State Chem.* **1971**, *3*, 1–11. [CrossRef]

92. Hosono, E.; Matsuda, H.; Honma, I.; Fujihara, S.; Ichihara, M.; Zhou, H. Synthesis of single crystalline electro-conductive $Na_{0.44}MnO_2$ nanowires with high aspect ratio for the fast charge–discharge Li ion battery. *J. Power Sources* **2008**, *182*, 349–352. [CrossRef]
93. Zhou, X.; Guduru, R.K.; Mohanty, P. Synthesis and characterization of $Na_{0.44}MnO_2$ from solution precursors. *J. Mater. Chem. A* **2013**, *1*, 2757–2761. [CrossRef]
94. Shen, K.-Y.; Lengyel, M.; Wang, L.; Axelbaum, R.L. Spray pyrolysis and electrochemical performance of $Na_{0.44}MnO_2$ for sodium-ion battery cathodes. *MRS Commun.* **2017**, *7*, 74–77. [CrossRef]
95. Zhang, J.; Yuan, H.; Huang, Y.; Kan, S.; Wu, Y.; Bu, M.; Liu, Y.; He, P.; Liu, H. Engineering sodium-rich manganese oxide with robust tunnel structure for high-performance sodium-ion battery cathode application. *Chem. Eng. J.* **2021**, *417*, 128097. [CrossRef]
96. Chae, M.S.; Elias, Y.; Aurbach, D. Tunnel-Type Sodium Manganese Oxide Cathodes for Sodium-Ion Batteries. *ChemElectroChem* **2021**, *8*, 798–811. [CrossRef]
97. Kim, D.J.; Ponraj, R.; Kannan, A.G.; Lee, H.-W.; Fathi, R.; Ruffo, R.; Mari, C.M.; Kim, D.K. Diffusion behavior of sodium ions in $Na_{0.44}MnO_2$ in aqueous and non-aqueous electrolytes. *J. Power Sources* **2013**, *244*, 758–763. [CrossRef]
98. He, X.; Wang, J.; Qiu, B.; Paillard, E.; Ma, C.; Cao, X.; Liu, H.; Stan, M.C.; Liu, H.; Gallash, T.; et al. Durable high-rate capability $Na_{0.44}MnO_2$ cathode material for sodium-ion batteries. *Nano Energy* **2016**, *27*, 602–610. [CrossRef]
99. Guo, S.; Yu, H.; Liu, D.; Tian, W.; Liu, X.; Hanada, N.; Ishida, M.; Zhou, H. A novel tunnel $Na_{0.6}1Ti_{0.48}Mn_{0.52}O_2$ cathode material for sodium-ion batteries. *Chem. Commun.* **2014**, *50*, 7998–8001. [CrossRef]
100. Xu, S.; Wang, Y.; Ben, L.; Lyu, Y.; Song, N.; Yang, Z.; Li, Y.; Mu, L.; Yang, H.-T.; Gu, L.; et al. Fe-Based Tunnel-Type $Na_{0.61}[Mn_{0.27}Fe_{0.34}Ti_{0.39}]O_2$ Designed by a New Strategy as a Cathode Material for Sodium-Ion Batteries. *Adv. Energy Mater.* **2015**, *5*, 1501156. [CrossRef]
101. Shi, W.-J.; Zheng, Y.-M.; Meng, X.-M.; Liu, S.-B.; Xu, S.-D.; Chen, L.; Wang, X.-M.; Zhang, D. Designing Sodium Manganese Oxide with 4 d-Cation Zr Doping as a High-Rate-Performance Cathode for Sodium-Ion Batteries. *ChemElectroChem* **2020**, *7*, 2545–2552. [CrossRef]
102. Zheng, P.; Su, J.; Wang, Y.; Zhou, W.; Song, J.; Su, Q.; Reeves-McLaren, N.; Guo, S. A High-Performance Primary Nanosheet Heterojunction Cathode Composed of $Na_{0.44}MnO_2$ Tunnels and Layered $Na_2Mn_3O_7$ for Na-Ion Batteries. *ChemSusChem* **2020**, *13*, 1793–1799. [CrossRef]
103. Zhou, Y.-T.; Sun, X.; Zou, B.-K.; Liao, J.-Y.; Wen, Z.-Y.; Chen, C.-H. Cobalt-substituted $Na_{0.44}Mn_{1-x}Co_xO_2$: Phase evolution and a high capacity positive electrode for sodium-ion batteries. *Electrochim. Acta* **2016**, *213*, 496–503. [CrossRef]
104. Han, D.-W.; Ku, J.-H.; Kim, R.-H.; Yun, D.-J.; Lee, S.-S.; Doo, S.-G. Aluminum Manganese Oxides with Mixed Crystal Structure: High-Energy-Density Cathodes for Rechargeable Sodium Batteries. *ChemSusChem* **2014**, *7*, 1870–1875. [CrossRef]
105. Tang, W.; Song, X.; Du, Y.; Peng, C.; Lin, M.; Xi, S.; Tian, B.; Zheng, J.; Wu, Y.; Pan, F.; et al. High-performance $NaFePO_4$ formed by aqueous ion-exchange and its mechanism for advanced sodium ion batteries. *J. Mater. Chem. A* **2016**, *4*, 4882–4892. [CrossRef]
106. Ling, M.; Lv, Z.; Li, F.; Zhao, J.; Zhang, H.; Hou, G.; Zheng, Q.; Li, X. Revisiting of Tetragonal $NaVPO_4F$: A High Energy Density Cathode for Sodium-Ion Batteries. *ACS Appl. Mater. Interfaces* **2020**, *12*, 30510–30519. [CrossRef] [PubMed]
107. Gutierrez, A.; Kim, S.; Fister, T.T.; Johnson, C.S. Microwave-Assisted Synthesis of $NaCoPO_4$ Red-Phase and Initial Characterization as High Voltage Cathode for Sodium-Ion Batteries. *ACS Appl. Mater. Interfaces* **2017**, *9*, 4391–4396. [CrossRef] [PubMed]
108. Priyanka, V.; Savithiri, G.; Subadevi, R.; Sivakumar, M. An emerging electrochemically active maricite $NaMnPO_4$ as cathode material at elevated temperature for sodium-ion batteries. *Appl. Nanosci.* **2020**, *10*, 3945–3951. [CrossRef]
109. Mathew, V.; Kim, S.; Kang, J.; Gim, J.; Song, J.; Baboo, J.P.; Park, W.; Ahn, D.; Han, J.; Gu, L.; et al. Amorphous iron phosphate: Potential host for various charge carrier ions. *NPG Asia Mater.* **2014**, *6*, e138. [CrossRef]
110. Wang, R.; Wu, S.; Zhang, F.; Zhao, X.; Lin, Z.; Wang, C.-Z.; Ho, K.-M. Stabilizing the crystal structures of $NaFePO_4$ with Li substitutions. *Phys. Chem. Chem. Phys.* **2020**, *22*, 13975–13980. [CrossRef]
111. Ali, G.; Lee, J.-H.; Susanto, D.; Choi, S.-W.; Cho, B.W.; Nam, K.-W.; Chung, K.Y. Polythiophene-Wrapped Olivine $NaFePO_4$ as a Cathode for Na-Ion Batteries. *ACS Appl. Mater. Interfaces* **2016**, *8*, 15422–15429. [CrossRef]
112. Priyanka, V.; Savithiri, G.; Rajkumar, P.; Meenatchi, T.; Subadevi, R.; Sivakumar, M. Tweaking the electrochemical activity of maricite $NaMnPO_4$ in sodium batteries using different manganese precursors via polyol method. *J. Solid. State Chem.* **2020**, *290*, 121551. [CrossRef]
113. Venkatachalam, P.; Ganesan, S.; Rengapillai, S.; Marimuthu, S. Gradual Development of Maricite $NaMnPO_4$ with the Influence of Diol Chain Length on the Polyol Process of Surpassed Sodium Intercalation. *Ind. Eng. Chem. Res.* **2021**, *60*, 5861–5868. [CrossRef]
114. Kosova, N.V.; Podugolnikov, V.R.; Devyatkina, E.T.; Slobodyuk, A.B. Structure and electrochemistry of $NaFePO_4$ and Na_2FePO_4F cathode materials prepared via mechanochemical route. *Mater. Res. Bull.* **2014**, *60*, 849–857. [CrossRef]
115. Jian, Z.; Yuan, C.; Han, W.; Lu, X.; Gu, L.; Xi, X.; Hu, Y.-S.; Li, H.; Chen, W.; Chen, D.; et al. Atomic Structure and Kinetics of NASICON $Na_xV_2(PO_4)_3$ Cathode for Sodium-Ion Batteries. *Adv. Funct. Mater.* **2014**, *24*, 4265–4272. [CrossRef]
116. Goodenough, J.B.; Hong, H.Y.P.; Kafalas, J.A. Fast Na^+-ion transport in skeleton structures. *Mater. Res. Bull.* **1976**, *11*, 203–220. [CrossRef]
117. Hong, H.Y.P. Crystal structures and crystal chemistry in the system $Na_{1+x}Zr_2Si_xP_{3-x}O_{12}$. *Mater. Res. Bull.* **1976**, *11*, 173–182. [CrossRef]

118. Oh, J.A.S.; He, L.; Plewa, A.; Morita, M.; Zhao, Y.; Sakamoto, T.; Song, X.; Zhai, W.; Zeng, K.; Lu, L. Composite NASICON ($Na_3Zr_2Si_2PO_{12}$) Solid-State Electrolyte with Enhanced Na+ Ionic Conductivity: Effect of Liquid Phase Sintering. *ACS Appl. Mater. Interfaces* **2019**, *11*, 40125–40133. [CrossRef]
119. Gopalakrishnan, J.; Rangan, K.K. Vanadium phosphate ($V_2(PO_4)_3$): A novel NASICO N-type vanadium phosphate synthesized by oxidative deintercalation of sodium from sodium vanadium phosphate ($Na_3V_2(PO_4)_3$). *Chem. Mater.* **1992**, *4*, 745–747. [CrossRef]
120. Zhu, Y.; Xu, H.; Ma, J.; Chen, P.; Chen, Y. The recent advances of NASICON-$Na_3V_2(PO_4)_3$ cathode materials for sodium-ion batteries. *J. Solid. State Chem.* **2023**, *317*, 123669. [CrossRef]
121. Pandit, B.; Sougrati, M.T.; Fraisse, B.; Monconduit, L. Exploration of a $Na_3V_2(PO_4)_3$/C-Pb full cell Na-ion prototype. *Nano Energy* **2022**, *95*, 107010. [CrossRef]
122. Zhang, X.; Rui, X.; Chen, D.; Tan, H.; Yang, D.; Huang, S.; Yu, Y. $Na_3V_2(PO_4)_3$: An advanced cathode for sodium-ion batteries. *Nanoscale* **2019**, *11*, 2556–2576. [CrossRef]
123. Song, W.; Cao, X.; Wu, Z.; Chen, J.; Huangfu, K.; Wang, X.; Huang, Y.; Ji, X. A study into the extracted ion number for NASICON structured $Na_3V_2(PO_4)_3$ in sodium-ion batteries. *Phys. Chem. Chem. Phys.* **2014**, *16*, 17681–17687. [CrossRef]
124. Cao, X.; Sun, Q.; Zhu, L.; Xie, L. $Na_3V_2(PO_4)_3$ nanoparticles confined in functional carbon framework towards high-rate and ultralong-life sodium storage. *J. Alloys Compd.* **2019**, *791*, 296–306. [CrossRef]
125. Lim, S.-J.; Han, D.-W.; Nam, D.-H.; Hong, K.-S.; Eom, J.-Y.; Ryu, W.-H.; Kwon, H.-S. Structural enhancement of $Na_3V_2(PO_4)_3$/C composite cathode materials by pillar ion doping for high power and long cycle life sodium-ion batteries. *J. Mater. Chem. A* **2014**, *2*, 19623–19632. [CrossRef]
126. Pal, S.K.; Thirupathi, R.; Chakrabarty, S.; Omar, S. Improving the Electrochemical Performance of $Na_3V_2(PO_4)_3$ Cathode in Na-Ion Batteries by Si-Doping. *ACS Appl. Energy Mater.* **2020**, *3*, 12054–12065. [CrossRef]
127. Chen, Y.; Cheng, J.; Wang, Y.; Wang, C.; He, Z.; Li, D.; Guo, L. Insights into the elevated electrochemical performance and kinetic characteristics of magnesium-substituted $Na_3V_{2-x}Mg_x(PO_4)_3$/C with superior rate capability and long lifespan. *J. Mater. Sci.* **2020**, *55*, 13141–13156. [CrossRef]
128. Song, W.; Liu, S. A sodium vanadium three-fluorophosphate cathode for rechargeable batteries synthesized by carbothermal reduction. *Solid. State Sci.* **2013**, *15*, 1–6. [CrossRef]
129. Song, W.; Wu, Z.; Chen, J.; Lan, Q.; Zhu, Y.; Yang, Y.; Pan, C.; Hou, H.; Jing, M.; Ji, X. High-voltage NASICON Sodium Ion Batteries: Merits of Fluorine Insertion. *Electrochim. Acta* **2014**, *146*, 142–150. [CrossRef]
130. Wei, P.; Chen, W.; Jing, Q.; Lee, M.-H.; Chen, Z. Effects of P_2O_7 clusters arrangement on second harmonic generation responses of pyrophosphates. *J. Alloys Compd.* **2020**, *827*, 153922. [CrossRef]
131. Niu, Y.; Zhang, Y.; Xu, M. A review on pyrophosphate framework cathode materials for sodium-ion batteries. *J. Mater. Chem. A* **2019**, *7*, 15006–15025. [CrossRef]
132. Uebou, Y.; Okada, S.; Yamaki, J.-I. Electrochemical insertion of lithium and sodium into $(MoO_2)_2P_2O_7$. *J. Power Sources* **2003**, *115*, 119–124. [CrossRef]
133. Gabelica-Robert, M.; Goreaud, M.; Labbe, P.; Raveau, B. The pyrophosphate $NaFeP_2O_7$: A cage structure. *J. Solid. State Chem.* **1982**, *45*, 389–395. [CrossRef]
134. Barpanda, P.; Lu, J.; Ye, T.; Kajiyama, M.; Chung, S.-C.; Yabuuchi, N.; Komaba, S.; Yamada, A. A layer-structured $Na_2CoP_2O_7$ pyrophosphate cathode for sodium-ion batteries. *RSC Adv.* **2013**, *3*, 3857–3860. [CrossRef]
135. Barpanda, P.; Ye, T.; Avdeev, M.; Chung, S.-C.; Yamada, A. A new polymorph of $Na_2MnP_2O_7$ as a 3.6 V cathode material for sodium-ion batteries. *J. Mater. Chem. A* **2013**, *1*, 4194–4197. [CrossRef]
136. Barpanda, P.; Liu, G.; Ling, C.D.; Tamaru, M.; Avdeev, M.; Chung, S.-C.; Yamada, Y.; Yamada, A. $Na_2FeP_2O_7$: A Safe Cathode for Rechargeable Sodium-ion Batteries. *Chem. Mater.* **2013**, *25*, 3480–3487. [CrossRef]
137. Kim, H.; Park, C.S.; Choi, J.W.; Jung, Y. Defect-Controlled Formation of Triclinic $Na_2CoP_2O_7$ for 4 V Sodium-Ion Batteries. *Angew. Chem. Int. Ed.* **2016**, *55*, 6662–6666. [CrossRef] [PubMed]
138. Ha, K.-H.; Woo, S.H.; Mok, D.; Choi, N.-S.; Park, Y.; Oh, S.M.; Kim, Y.; Kim, J.; Lee, J.; Nazar, L.F.; et al. $Na_{4-\alpha}M_{2+\alpha/2}(P_2O_7)_2$ ($2/3 \leq \alpha \leq 7/8$, M = Fe, $Fe_{0.5}Mn_{0.5}$, Mn): A Promising Sodium Ion Cathode for Na-ion Batteries. *Adv. Energy Mater.* **2013**, *3*, 770–776. [CrossRef]
139. Erragh, F.; Boukhari, A.; Abraham, F.; Elouadi, B. Study of the Crystal Structures of Sodium Magnesium and Sodium Nickel Diphosphates. *J. Solid. State Chem.* **2000**, *152*, 323–331. [CrossRef]
140. Liu, G.; Nishimura, S.-I.; Chung, S.C.; Fujii, K.; Yashima, M.; Yamada, A. Defect induced sodium disorder and ionic conduction mechanism in $Na_{1.82}Mg_{1.09}P_2O_7$. *J. Mater. Chem. A* **2014**, *2*, 18353–18359. [CrossRef]
141. Kim, H.; Shakoor, R.A.; Park, C.; Lim, S.Y.; Kim, J.-S.; Jo, Y.N.; Cho, W.; Miyasaka, K.; Kahraman, R.; Jung, Y.; et al. $Na_2FeP_2O_7$ as a Promising Iron-Based Pyrophosphate Cathode for Sodium Rechargeable Batteries: A Combined Experimental and Theoretical Study. *Adv. Funct. Mater.* **2013**, *23*, 1147–1155. [CrossRef]
142. Liu, H.; Zhao, Y.; Zhang, H.; Lian, X.; Dong, Y.; Kuang, Q. Structural and electrochemical properties of Fe-doped $Na_2Mn_{3-x}Fe_x(P_2O_7)_2$ cathode material for sodium ion batteries. *J. Power Sources* **2017**, *370*, 114–121. [CrossRef]
143. Kumar, S.; Singh, M.; Mondal, R.; Kumar, M.; Prakash, R.; Singh, P. $Mo_2P_2O_{11}$: A Potential Cathode Material for Rechargeable Sodium-Ion Batteries. *Energy Fuels* **2023**, *37*, 1288–1296. [CrossRef]
144. Pu, X.; Wang, H.; Yuan, T.; Cao, S.; Liu, S.; Xu, L.; Yang, H.; Ai, X.; Chen, Z.; Cao, Y. $Na_4Fe_3(PO_4)_2P_2O_7$/C nanospheres as low-cost, high-performance cathode material for sodium-ion batteries. *Energy Stor. Mater.* **2019**, *22*, 330–336. [CrossRef]

145. Kundu, D.; Tripathi, R.; Popov, G.; Makahnouk, W.R.M.; Nazar, L.F. Synthesis, Structure, and Na-Ion Migration in $Na_4NiP_2O_7F_2$: A Prospective High Voltage Positive Electrode Material for the Na-Ion Battery. *Chem. Mater.* **2015**, *27*, 885–891. [CrossRef]
146. Masese, T.; Orikasa, Y.; Tassel, C.; Kim, J.; Minato, T.; Arai, H.; Mori, T.; Yamamoto, K.; Kobayashi, Y.; Kageyama, H.; et al. Relationship between Phase Transition Involving Cationic Exchange and Charge-Discharge Rate in Li_2FeSiO_4. *Chem. Mater.* **2014**, *26*, 1380–1384. [CrossRef]
147. Gao, S.; Zhao, J.; Zhao, Y.; Wu, Y.; Zhang, X.; Wang, L.; Liu, X.; Rui, Y.; Xu, J. Na_2CoSiO_4 as a novel positive electrode material for sodium-ion capacitors. *Mater. Lett.* **2015**, *158*, 300–303. [CrossRef]
148. Treacher, J.C.; Wood, S.M.; Islam, M.S.; Kendrick, E. Na_2CoSiO_4 as a cathode material for sodium-ion batteries: Structure, electrochemistry and diffusion pathways. *Phys. Chem. Chem. Phys.* **2016**, *18*, 32744–32752. [CrossRef]
149. Wang, J.; Hoteling, G.; Shepard, R.; Wahila, M.; Wang, F.; Smeu, M.; Liu, H. Reaction Mechanism of Na-Ion Deintercalation in Na_2CoSiO_4. *J. Phys. Chem. C* **2022**, *126*, 16983–16992. [CrossRef]
150. Pedone, A.; Malavasi, G.; Menziani, M.C.; Cormack, A.N.; Segre, U. A New Self-Consistent Empirical Interatomic Potential Model for Oxides, Silicates, and Silica-Based Glasses. *J. Phys. Chem. B* **2006**, *110*, 11780–11795. [CrossRef]
151. Wu, P.; Wu, S.Q.; Lv, X.; Zhao, X.; Ye, Z.; Lin, Z.; Wang, C.Z.; Ho, K.M. Fe–Si networks in Na_2FeSiO_4 cathode materials. *Phys. Chem. Chem. Phys.* **2016**, *18*, 23916–23922. [CrossRef]
152. Bianchini, F.; Fjellvåg, H.; Vajeeston, P. First-principles study of the structural stability and electrochemical properties of Na_2MSiO_4 (M = Mn, Fe, Co and Ni) polymorphs. *Phys. Chem. Chem. Phys.* **2017**, *19*, 14462–14470. [CrossRef]
153. Jin, T.; Li, H.; Zhu, K.; Wang, P.-F.; Liu, P.; Jiao, L. Polyanion-type cathode materials for sodium-ion batteries. *Chem. Soc. Rev.* **2020**, *49*, 2342–2377. [CrossRef]
154. Kee, Y.; Dimov, N.; Staykov, A.; Okada, S. Investigation of metastable Na_2FeSiO_4 as a cathode material for Na-ion secondary battery. *Mater. Chem. Phys.* **2016**, *171*, 45–49. [CrossRef]
155. Rangasamy, V.S.; Thayumanasundaram, S.; Locquet, J.-P. Solvothermal synthesis and electrochemical properties of Na_2CoSiO_4 and Na_2CoSiO_4/carbon nanotube cathode materials for sodium-ion batteries. *Electrochim. Acta* **2018**, *276*, 102–110. [CrossRef]
156. Guan, W.H.; Lin, Q.Y.; Lan, Z.Y.; Pan, W.L.; Wei, X.; Sun, W.P.; Zheng, R.T.; Lu, Y.H.; Shu, J.; Pan, H.G.; et al. Approaching the theoretical capacity limit of Na_2FeSiO_4-based cathodes with fully reversible two-electron redox reaction for sodium-ion battery. *Mater. Today Nano* **2020**, *12*, 100098. [CrossRef]
157. Law, M.; Ramar, V.; Balaya, P. Na_2MnSiO_4 as an attractive high capacity cathode material for sodium-ion battery. *J. Power Sources* **2017**, *359*, 277–284. [CrossRef]
158. Schon, T.B.; McAllister, B.T.; Li, P.-F.; Seferos, D.S. The rise of organic electrode materials for energy storage. *Chem. Soc. Rev.* **2016**, *45*, 6345–6404. [CrossRef] [PubMed]
159. Wang, H.-G.; Yuan, S.; Ma, D.-L.; Huang, X.-L.; Meng, F.-L.; Zhang, X.-B. Tailored Aromatic Carbonyl Derivative Polyimides for High-Power and Long-Cycle Sodium-Organic Batteries. *Adv. Energy Mater.* **2014**, *4*, 1301651. [CrossRef]
160. Wang, S.; Wang, L.; Zhu, Z.; Hu, Z.; Zhao, Q.; Chen, J. All Organic Sodium-Ion Batteries with $Na_4C_8H_2O_6$. *Angew. Chem.* **2014**, *126*, 6002–6006. [CrossRef]
161. Kim, H.; Kwon, J.E.; Lee, B.; Hong, J.; Lee, M.; Park, S.Y.; Kang, K. High Energy Organic Cathode for Sodium Rechargeable Batteries. *Chem. Mater.* **2015**, *27*, 7258–7264. [CrossRef]
162. Shen, Y.F.; Yuan, D.D.; Ai, X.P.; Yang, H.X.; Zhou, M. Poly(diphenylaminesulfonic acid sodium) as a cation-exchanging organic cathode for sodium batteries. *Electrochem. Commun.* **2014**, *49*, 5–8. [CrossRef]
163. Wang, C.; Xu, Y.; Fang, Y.; Zhou, M.; Liang, L.; Singh, S.; Zhao, H.; Schober, A.; Lei, Y. Extended π-Conjugated System for Fast-Charge and -Discharge Sodium-Ion Batteries. *J. Am. Chem. Soc.* **2015**, *137*, 3124–3130. [CrossRef]
164. Han, S.C.; Bae, E.G.; Lim, H.; Pyo, M. Non-crystalline oligopyrene as a cathode material with a high-voltage plateau for sodium ion batteries. *J. Power Sources* **2014**, *254*, 73–79. [CrossRef]
165. Sakaushi, K.; Hosono, E.; Nickerl, G.; Gemming, T.; Zhou, H.; Kaskel, S.; Eckert, J. Aromatic porous-honeycomb electrodes for a sodium-organic energy storage device. *Nat. Commun.* **2013**, *4*, 1485. [CrossRef]
166. Wang, D.-Y.; Liu, R.; Guo, W.; Li, G.; Fu, Y. Recent advances of organometallic complexes for rechargeable batteries. *Coord. Chem. Rev.* **2021**, *429*, 213650. [CrossRef]
167. Zhao, R.; Liang, Z.; Zou, R.; Xu, Q. Metal-Organic Frameworks for Batteries. *Joule* **2018**, *2*, 2235–2259. [CrossRef]
168. Li, X.; Yang, X.; Xue, H.; Pang, H.; Xu, Q. Metal–organic frameworks as a platform for clean energy applications. *EnergyChem* **2020**, *2*, 100027. [CrossRef]
169. Du, M.; Li, Q.; Zhao, Y.; Liu, C.-S.; Pang, H. A review of electrochemical energy storage behaviors based on pristine metal–organic frameworks and their composites. *Coord. Chem. Rev.* **2020**, *416*, 213341. [CrossRef]
170. Lu, Y.; Wang, L.; Cheng, J.; Goodenough, J.B. Prussian blue: A new framework of electrode materials for sodium batteries. *Chem. Commun.* **2012**, *48*, 6544–6546. [CrossRef] [PubMed]
171. Yi, H.; Qin, R.; Ding, S.; Wang, Y.; Li, S.; Zhao, Q.; Pan, F. Structure and Properties of Prussian Blue Analogues in Energy Storage and Conversion Applications. *Adv. Funct. Mater.* **2020**, *31*, 2006970. [CrossRef]
172. Luo, Y.; Peng, J.; Yin, S.; Xue, L.; Yan, Y. Acid-Assisted Ball Mill Synthesis of Carboxyl-Functional-Group-Modified Prussian Blue as Sodium-Ion Battery Cathode. *Nanomaterials* **2022**, *12*, 1290. [CrossRef]
173. Xie, B.X.; Sun, B.Y.; Gao, T.Y.; Ma, Y.L.; Yin, G.P.; Zuo, P.J. Recent progress of Prussian blue analogues as cathode materials for nonaqueous sodium-ion batteries. *Coord. Chem. Rev.* **2022**, *460*, 214478. [CrossRef]

174. Fu, H.; Liu, C.; Zhang, C.; Ma, W.; Wang, K.; Li, Z.; Lu, X.; Cao, G. Enhanced storage of sodium ions in Prussian blue cathode material through nickel doping. *J. Mater. Chem. A* **2017**, *5*, 9604–9610. [CrossRef]
175. Qian, J.F.; Zhou, M.; Cao, Y.L.; Ai, X.P.; Yang, H.X. Nanosized $Na_4Fe(CN)_6$/C Composite as a Low-Cost and High-Rate Cathode Material for Sodium-Ion Batteries. *Adv. Energy Mater.* **2012**, *2*, 410–414. [CrossRef]
176. Li, W.-J.; Chou, S.-L.; Wang, J.-Z.; Kang, Y.-M.; Wang, J.-L.; Liu, Y.; Gu, Q.-F.; Liu, H.-K.; Dou, S.-X. Facile Method To Synthesize Na-Enriched $Na_{1+x}FeFe(CN)_6$ Frameworks as Cathode with Superior Electrochemical Performance for Sodium-Ion Batteries. *Chem. Mater.* **2015**, *27*, 1997–2003. [CrossRef]
177. Yang, D.; Liao, X.-Z.; Huang, B.; Shen, J.; He, Y.-S.; Ma, Z.-F. A $Na_4Fe(CN)_6$/NaCl solid solution cathode material with an enhanced electrochemical performance for sodium ion batteries. *J. Mater. Chem. A* **2013**, *1*, 13417–13421. [CrossRef]
178. Jiao, S.; Tuo, J.; Xie, H.; Cai, Z.; Wang, S.; Zhu, J. The electrochemical performance of $Cu_3[Fe(CN)_6]_2$ as a cathode material for sodium-ion batteries. *Mater. Res. Bull.* **2017**, *86*, 194–200. [CrossRef]
179. Sun, H.; Sun, H.; Wang, W.; Jiao, H.; Jiao, S. $Fe_4[Fe(CN)_6]_3$: A cathode material for sodium-ion batteries. *RSC Adv.* **2014**, *4*, 42991–42995. [CrossRef]
180. Matsuda, T.; Takachi, M.; Moritomo, Y. A sodium manganese ferrocyanide thin film for Na-ion batteries. *Chem. Commun.* **2013**, *49*, 2750–2752. [CrossRef]
181. Wang, L.; Lu, Y.; Liu, J.; Xu, M.; Cheng, J.; Zhang, D.; Goodenough, J.B. A Superior Low-Cost Cathode for a Na-Ion Battery. *Angew. Chem. Int. Ed.* **2013**, *52*, 1964–1967. [CrossRef]
182. Chen, Z.-Y.; Fu, X.-Y.; Zhang, L.-L.; Yan, B.; Yang, X.-L. High-Performance Fe-Based Prussian Blue Cathode Material for Enhancing the Activity of Low-Spin Fe by Cu Doping. *ACS Appl. Mater. Interfaces* **2022**, *14*, 5506–5513. [CrossRef]
183. Song, J.; Wang, L.; Lu, Y.; Liu, J.; Guo, B.; Xiao, P.; Lee, J.J.; Yang, X.Q.; Henkelman, G.; Goodenough, J.B. Removal of interstitial H_2O in hexacyanometallates for a superior cathode of a sodium-ion battery. *J. Am. Chem. Soc.* **2015**, *137*, 2658–2664. [CrossRef]
184. Hu, P.; Peng, W.; Wang, B.; Xiao, D.; Ahuja, U.; Réthoré, J.; Aifantis, K.E. Concentration-Gradient Prussian Blue Cathodes for Na-Ion Batteries. *ACS Energy Lett.* **2020**, *5*, 100–108. [CrossRef]
185. Xu, Z.; Sun, Y.; Xie, J.; Nie, Y.; Xu, X.W.; Tu, J.; Zhang, J.; Qiu, L.C.; Zhu, T.J.; Zhao, X.B. Scalable Preparation of Mn/Ni Binary Prussian Blue as Sustainable Cathode for Harsh-Condition-Tolerant Sodium-Ion Batteries. *ACS Sustain. Chem. Eng.* **2022**, *10*, 13277–13287. [CrossRef]
186. Nguyen, T.P.; Kim, I.T. Vanadium Ferrocyanides as a Highly Stable Cathode for Lithium-Ion Batteries. *Molecules* **2023**, *28*, 461. [CrossRef] [PubMed]
187. Pan, Z.T.; He, Z.H.; Hou, J.F.; Kong, L.B. Sodium vanadium hexacyanoferrate as a high-rate capability and long-life cathode material for Na-ion batteries. *J. Energy Storage* **2022**, *53*, 105165. [CrossRef]
188. Noor, N.; Parkin, I.P. Enhanced transparent-conducting fluorine-doped tin oxide films formed by Aerosol-Assisted Chemical Vapour Deposition. *J. Mater. Chem. C* **2013**, *1*, 984–996. [CrossRef]
189. Wu, X.; Wu, C.; Wei, C.; Hu, L.; Qian, J.; Cao, Y.; Ai, X.; Wang, J.; Yang, H. Highly Crystallized $Na_2CoFe(CN)_6$ with Suppressed Lattice Defects as Superior Cathode Material for Sodium-Ion Batteries. *ACS Appl. Mater. Interfaces* **2016**, *8*, 5393–5399. [CrossRef]
190. Takachi, M.; Matsuda, T.; Moritomo, Y. Cobalt Hexacyanoferrate as Cathode Material for Na^+ Secondary Battery. *Appl. Phys. Express* **2013**, *6*, 025802. [CrossRef]
191. Baster, D.; Kondracki, L.; Oveisi, E.; Trabesinger, S.; Girault, H.H. Prussian Blue Analogue-Sodium-Vanadium Hexacyanoferrate as a Cathode Material for Na-Ion Batteries. *Acs Appl. Energy Mater.* **2021**, *4*, 9758–9765. [CrossRef]
192. Nguyen, T.P.; Kim, I.T. Iron-Vanadium Incorporated Ferrocyanides as Potential Cathode Materials for Application in Sodium-Ion Batteries. *Micromachines* **2023**, *14*, 521. [CrossRef]
193. Zhang, Y.; Yang, S.; Chang, X.; Guo, H.; Li, Y.; Wang, M.; Li, W.; Jiao, L.; Wang, Y. MOF based on a longer linear ligand: Electrochemical performance, reaction kinetics, and use as a novel anode material for sodium-ion batteries. *Chem. Commun.* **2018**, *54*, 11793–11796. [CrossRef]
194. Férey, G.; Millange, F.; Morcrette, M.; Serre, C.; Doublet, M.-L.; Grenèche, J.-M.; Tarascon, J.-M. Mixed-Valence Li/Fe-Based Metal–Organic Frameworks with Both Reversible Redox and Sorption Properties. *Angew. Chem. Int. Ed.* **2007**, *46*, 3259–3263. [CrossRef]
195. Chen, T.; Liu, X.; Niu, L.; Gong, Y.; Li, C.; Xu, S.; Pan, L. Recent progress on metal–organic framework-derived materials for sodium-ion battery anodes. *Inorg. Chem. Front.* **2020**, *7*, 567–582. [CrossRef]
196. Li, H.; Wang, T.; Wang, X.; Li, G.; Shen, J.; Chai, J. MOF-derived Al-doped Na_2FePO_4F/mesoporous carbon nanonetwork composites as high-performance cathode material for sodium-ion batteries. *Electrochim. Acta* **2021**, *373*, 137905. [CrossRef]
197. Yu, T.-Y.; Sun, Y.-K. A fluorinated O_3-type layered cathode for long-life sodium-ion batteries. *J. Mater. Chem. A* **2022**, *10*, 23639–23648. [CrossRef]
198. Zhou, Q.; Wang, L.; Li, W.; Zhao, K.; Liu, M.; Wu, Q.; Yang, Y.; He, G.; Parkin, I.P.; Shearing, P.R.; et al. Sodium Superionic Conductors (NASICONs) as Cathode Materials for Sodium-Ion Batteries. *Electrochem. Energy Rev.* **2021**, *4*, 793–823. [CrossRef]
199. Wang, Q.; Wu, X.; You, H.; Min, H.; Xu, X.; Hao, J.; Liu, X.; Yang, H. Template-directed Prussian blue nanocubes supported on Ni foam as the binder-free anode of lithium-ion batteries. *Appl. Surf. Sci.* **2022**, *571*, 151194. [CrossRef]
200. Kim, H.; Sadan, M.K.; Kim, C.; Jo, J.; Seong, M.; Cho, K.-K.; Kim, K.-W.; Ahn, J.-H.; Ahn, H.-J. Enhanced reversible capacity of sulfurized polyacrylonitrile cathode for room-temperature Na/S batteries by electrochemical activation. *Chem. Eng. J.* **2021**, *426*, 130787. [CrossRef]

201. Huang, Z.-X.; Zhang, X.-L.; Zhao, X.-X.; Zhao, Y.-Y.; Aravindan, V.; Liu, Y.-H.; Geng, H.; Wu, X.-L. Electrode/electrolyte additives for practical sodium-ion batteries: A mini review. *Inorg. Chem. Front.* **2023**, *10*, 37–48. [CrossRef]
202. Hou, Y.; Jin, J.; Huo, C.; Liu, Y.; Deng, S.; Chen, J. New insights into the critical role of inactive element substitution in improving the rate performance of sodium oxide cathode material. *Energy Stor. Mater.* **2023**, *56*, 87–95. [CrossRef]
203. Nanba, Y.; Iwao, T.; Boisse, B.M.D.; Zhao, W.; Hosono, E.; Asakura, D.; Niwa, H.; Kiuchi, H.; Miyawaki, J.; Harada, Y.; et al. Redox Potential Paradox in Na_xMO_2 for Sodium-Ion Battery Cathodes. *Chem. Mater.* **2016**, *28*, 1058–1065. [CrossRef]